Logarithmic theory of visuomotor stabilization

Leonardo Demarchi *
Sorbonne Université, CNRS, Laboratoire Jean Perrin, LJP, F75005 Paris, France
and Sorbonne Université, CNRS, Inserm, Institut de Biologie Paris-Seine, IBPS, F75005 Paris, France

(Received 21 November 2025; accepted 27 January 2026; published 8 April 2026)

Although many animals rely on visual information to navigate, optic flow is inherently ambiguous as it confounds information about motion speed and object distance. As a result, the visual feedback produced by a given motor command is context dependent and requires an appropriately adapted response. Recent experiments have investigated how the fish *Danionella cerebrum* use visual cues to stabilize their position against simulated external currents. Logarithmic sensorimotor transformations have been proposed to enable adaptive responses to perturbations while preventing delay-induced instabilities. Here, we develop the theoretical framework introduced for continuous locomotion to show how logarithmic coding naturally gives rise to this adaptive behavior. The system is modeled by a nonlinear delay differential equation, which is analyzed using dynamical systems theory. We further analyze experimental data to uncover the mechanisms underlying swimming initiation and positional drift correction. Finally, we extend our framework to intermittent locomotion, resulting in a nonlinear difference equation, and show that it still produces robust adaptive behavior. This is motivated by the literature on zebrafish, where visuomotor stabilization has been extensively studied, but burst-and-coast swimming obscures the underlying adaptation mechanism. We show that our theory can reproduce the experimental results reported for motor adaptation in zebrafish without invoking internal models. Overall, our results highlight logarithmic coding as a unifying principle for visuomotor stability across continuous and intermittent locomotor regimes.

DOI: 10.1103/2s81-6lr6

I. INTRODUCTION

Vision is widespread in the animal kingdom, as it provides individuals with detailed information about their surroundings, important for survival and reproduction [1]. In particular, it plays a central role in guiding locomotion and spatial navigation [2]. While navigating complex environments, animals must continuously adapt their behavior to external perturbations in order to maintain their course. This is a difficult task, as sensory inputs only give a limited and noisy view of the state of the body and the environment, and motor actions are hindered by finite temporal delays [3]. These challenges are not unique to biology; they are also faced by engineers designing robotic systems capable of operating in real-world scenarios [4]. One approach that has emerged as a common solution, and is employed by animals and robots in multiple contexts, is the implementation of forward internal models—that is, the ability to use current motor commands to predict future sensory inputs [5–8]. Such models enable organisms to anticipate delays and adapt their behavior by using measured sensory inputs to minimize prediction errors, thereby maintaining accurate internal predictions across varying contexts. Although powerful, this approach is computationally demanding, suggesting that evolution may have found simpler mechanisms to achieve robust adaptation for basic problems common across species.

An example of such a common problem is that of stabilizing one's position against external currents while navigating through a fluid. As an animal moves relative to its environment, the visual scene it perceives changes over time. The resulting apparent motion of the surrounding objects, called optic flow, is an important visual cue used to guide locomotion [9,10]. While terrestrial animals like humans generally rely on friction with the ground to maintain stability, flying and swimming animals must continually adjust their movements to avoid being carried away by air or water currents. In these cases, vision is crucial for remaining stable relative to the surroundings, as any displacement produces a corresponding optic flow [11,12]. Thus, these organisms share the challenge of using visual inputs to modulate their thrust and counteract the effect of external perturbations.

In neuroscience, a common experimental paradigm is to present visual stimuli that simulate such whole-field motion of the animal. In these settings, the animals reliably respond by moving in a way that compensates for the apparent perturbation, a behavior known as the optomotor response [13,14]. In recent years, larval zebrafish has been used extensively as a model to study this behavior [15–17], as their small size and transparency allow for functional whole-brain imaging at cellular resolution, making it possible to investigate the neural circuits involved [18,19]. However, researchers do not agree on the underlying computations performed by this animal. Some have proposed that the fish perform motor learning using a forward internal model [20,21], or even that

*Contact author: leonardo.demarchi@sorbonne-universite.fr

they encode a memory of their location in the environment [22]. Others have proposed alternative mechanisms based on simpler feedback controllers [23–25], but these models are usually designed to explain data from individual experiments, disregarding prior findings. The difficulty mainly arises from the fact that zebrafish swim intermittently in discrete bouts, allowing them to independently adjust the intensity and timing of each bout to achieve the same average speed. As a result, the problem of stabilization through intermittent locomotion is underdetermined, making it challenging to identify the underlying sensorimotor computations.

A different animal model, the miniature fish *Danionella cerebrum* [26,27], is emerging as an alternative to zebrafish. It remains small and transparent at the adult stage, such that brain imaging can still be performed [28] while also permitting the study of a broader range of behaviors [29–33]. Another advantage of this model is that, at the larval stage, it swims continuously [34], making it much easier to study visuomotor stabilization by simply tracking the modulations of swimming speed over time. In fact, recent experiments have shown that the apparent adaptive behavior observed during visuomotor stabilization does not result from an internal model, but rather arises from the presence of nonlinear sensorimotor transformations [35]. These transformations correspond to the logarithmic encoding of both sensory input and motor output, which are well-known features of the sensory (Weber-Fechner law) and motor (Henneman's size principle) ends of the nervous system [36,37], suggesting that the resulting adaptive stabilization may be common to other species. By extending this model to the case of intermittent locomotion, we show that it can account for the adaptive behavior observed in zebrafish without invoking internal models or restricting the analysis to individual experimental results.

In Sec. II, we first introduce the translational optomotor response and review the literature on zebrafish by summarizing the findings of studies investigating this behavior. Then, in Sec. III, we revisit the recent experiments in danionella and analyze the mathematical framework proposed for visuomotor stabilization in the case of continuous locomotion. We also examine the initiation of swimming in response to external currents and an additional integration mechanism that prevents positional drift. Finally, in Sec. IV, we extend this framework to the case of intermittent locomotion, to study the stabilization process in zebrafish. We show that, even in this case, logarithmic coding leads to an emergent adaptation, preventing the instabilities that could arise from a delayed response to incomplete sensory information.

II. TRANSLATIONAL OPTOMOTOR RESPONSE

A. Quantification of optic flow

We begin by discussing in more detail what optic flow is and how to quantify it, since it is the feature of visual input that is relevant for the stabilization behavior studied in the rest of the paper. In the absence of mechanisms for depth estimation, the visual inputs available to the animal consist of information about the distribution of light as a function of its direction with respect to the eye. When an object moves relative to the animal, the angular position of its image on the retina changes. The optic flow refers to the angular velocity of the images moving across the retina. It can be quantified as the ratio between the component of the object velocity perpendicular to the line of sight and the distance of the object from the observer [9].

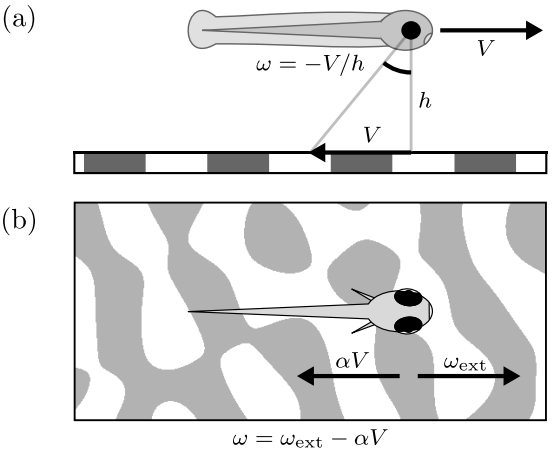

FIG. 1. Translational optic flow during fish locomotion. (a) A fish, moving forward with speed V relative to a stationary visual pattern at distance h, experiences a backward optic flow with characteristic angular velocity ω. (b) The total optic flow rate ω results from a forward component ω_{ext}, corresponding to the backward drift caused by a water current, and a backward component $-\alpha V$, corresponding to the visual feedback due to forward swimming.

Consider a fish moving forward with speed V at a distance h from a planar visual pattern [Fig. 1(a)]. In the reference frame that moves with fish, the pattern moves backward with the same speed V. Different points on the pattern will move differently across the retina, because of their different distances and directions, giving rise to a specific form of translational optic flow that reflects the specific geometry of the environment. We will only consider translational movements of such a planar pattern along the fish heading direction, therefore we can characterize the intensity and direction of the optic flow with the optic flow rate $\omega = -V/h$ [24]. This is simply the ratio between the velocity of the pattern and its distance, corresponding to the maximum possible angular velocity, which would be attained by the point located directly below the fish. We take it to be positive when the pattern moves forward with respect to the fish and negative when it moves backward. Importantly, we note that changing both the speed and the distance of the pattern by the same factor results in the same optic flow rate.

Now, if we externally translate the pattern it will give rise to the same optic flow as if it was the fish that was moving, but in the opposite direction. When we move the pattern forward with an external flow rate $\omega_{\text{ext}} > 0$, it corresponds to a backward movement of the fish. This visual stimulus is known to elicit an optomotor response, whereby animals actively move forward to counteract the effect of this fictive backward current. When the fish moves forward with speed V it experiences a backward optic flow with a rate proportional to its speed $-\alpha V$. We indicated the feedback gain α in place of the reciprocal pattern distance $1/h$ because certain experiments make it possible to manipulate the feedback and

thus disentangle it from the pattern distance. The overall optic flow rate is then given by the sum of these two contributions $\omega = \omega_{\text{ext}} - \alpha V$ [Fig. 1(b)].

B. Experiments in zebrafish larvae

There have been several studies investigating the translational optomotor response in the larval zebrafish, as its small size and transparency allow the use of imaging techniques to investigate the underlying neural circuits [15,17]. Mainly three different experimental approaches have been used to probe this behavior. In all cases the fish is positioned in a water tank and a visual pattern is displayed below it and translated to simulate the presence of an external water current. In the first approach (freely swimming), the fish are free to move and naturally experience the visual feedback resulting from their motion with respect to the visual pattern. In the second approach (head-restrained), the fish are embedded in an agarose gel in such a way that they can move their tail but their head remains stuck in place. A camera is used to record the tail movements and estimate what would be the corresponding forward motion of the fish. The visual pattern is updated accordingly in real time to restore the visual feedback in this restrained condition. In this way, one can choose the feedback gain α, which determines the intensity of the visual feedback for a given estimate of the speed, which is equivalent to choosing the pattern distance h in the freely swimming condition. The third approach (paralyzed) is similar to the second, except that the fish are paralyzed, and their intended movements are inferred from electrode recordings of motor nerve activity in their tail.

The first study quantifying how these fish can stabilize their position on average against external currents was Ref. [38]. The authors performed experiments with the freely swimming approach and varied the external flow rate across a broad range $\omega_{\text{ext}} = 0.2$–$8\,\text{rad/s}$, while the feedback gain was fixed by the distance of the visual pattern at $\alpha = 2\,\text{cm}^{-1}$. They observed that the fish adapted their average speed up to $\approx 2\,\text{cm/s}$ to match that of the external current. This adaptation resulted from an increasing bout speed V_{b}, an increasing bout duration T_{b} and a decreasing interbout duration T_{i} as ω_{ext} is increased. They also noted how the reaction time T_{r} between the onset of the current and the initiation of swimming decreased with ω_{ext}. Finally, they performed experiments in head-restrained conditions, but did not observe perfect stabilization, they reported significantly larger values of both T_{b} and T_{i}.

References [20,21] restrained the fish to easily manipulate the visual feedback, and studied how their behavior progressively changed after perturbations of the feedback gain. They presented fish with external currents with flow rate $\omega_{\text{ext}} = 2\,\text{rad/s}$ and switched between three different values of the feedback gain α. They did not quantify whether the fish stabilized their position with respect to the visual pattern. The authors of Ref. [20] used the head-restrained approach and found that, after increasing α, the duration of swimming bouts T_{b} decreased and the interbout duration T_{i} increased, with these changes manifesting gradually over several seconds. The authors of Ref. [21] used the paralyzed approach and found that, after increasing α, the bout speed V_{b} decreased over a few bouts and converged to a different value. They also observed a lower rate of swimming bouts $f_{\text{b}} = 1/(T_{\text{b}} + T_{\text{i}})$ for larger α. Both Refs. [20,21] proposed that fish maintain an internal representation of the relationship between motor command and visual feedback, updated through motor learning by comparing predicted and observed feedback.

Reference [39] studied the reaction times of fish to external currents using the head-restrained approach. The authors argued that swimming initiation follows a Poisson process, in which the fish can start swimming at any time with a rate dependent on ω_{ext}, as opposed to an evidence accumulation process in which the fish integrate the flow rate and start swimming when a threshold is reached.

Reference [23] introduced a feedback controller to describe the response of the fish to perturbations, again using the head-restrained approach. The authors perturbed the visual feedback corresponding to each swimming bout in a randomized fashion, either choosing different values of the feedback gain α, delaying the feedback by different times, or suppressing it completely in certain phases of the bout. They found the speed profile at the beginning of the swimming bout to be independent of the perturbations, which only resulted in a modulation of the final part of the bout, after a delay of $\approx 200\,\text{ms}$. They modeled the swimming initiation and termination with a feedback controller and used it to fit the observed bout and interbout durations $T_{\text{b,i}}$. The model does not account for changes of the swimming speed, but only for the timing of the swimming bouts based on the value of a motor drive with respect to a state-dependent threshold. The motor drive is given by the difference between the leaky integration of the net flow rate and that of the motor output, respectively modeling the integration of the sensory input and a process of motor inhibition.

Reference [24] used three different distances of the visual pattern to manipulate the visual feedback in freely swimming conditions. The authors noted that the speed during bouts followed the same temporal profile once renormalized by the initial speed. They found that fish adapted their swimming speed to that of the current, but did not match it exactly, resulting in imperfect stabilization. The bout speed V_{b} increased with ω_{ext} and decreased with α, while the bout rate f_{b} increased with ω_{ext} and was independent of α. They fitted the dependence of V_{b} and f_{b} using a feedback controller built upon the models of Refs. [39,23]. Bout initiation was modeled as a Poisson process with a rate proportional to the instantaneous forward flow rate and modulated by motor inhibition, whereas bout speed was controlled by the leaky integration of the forward flow rate.

Reference [22] proposed that the fish maintain a memory of their location in the environment, from experiments with the paralyzed approach. The authors presented fish with brief currents in open-loop conditions ($\alpha = 0$), directed either forward or backward, and followed, after a short pause, by a forward current in closed-loop conditions ($\alpha > 0$). They found that fish adapted their fictive swimming in the closed-loop phase to stabilize their position, compensating for the simulated displacement in the open-loop phase. The observed trajectories are compatible with a feedback controller that keeps the integrated net flow rate close to zero.

Reference [25] reproduced the experiments of Ref. [22] with the head-restrained approach. They varied the pauses between the two phases, finding that the swimming speed in the closed-loop phase remained significantly different for forward and backward open-loop currents, even after a pause of 16 s. They also tested a protocol in which a closed-loop current was followed by an open-loop one, finding that, for a given number of bouts in the closed-loop phase, the swimming speed during the open-loop phase was independent of α. They argued that fish can separate the external visual flow from the feedback, only using the former to regulate their speed, which implies the use of an internal model. Finally, they performed another experiment where they showed an open-loop current with a randomly switching direction, finding that the bout-triggered average stimulus decays exponentially with a time constant of $\approx$3 s. They reproduced these results using a model where swimming bouts are generated by a Poisson process with a time-varying rate. The rate was derived from leaky integration of the external flow rate, with a larger time constant in the absence of visual flow.

It is apparent that the experimental results and theoretical interpretations are not always compatible across different papers. On the experimental side, some of the inconsistencies might be due to different experimental conditions and approaches used to study the behavior. Some papers report that the fish can stabilize their position exactly, while others suggest that the regulation is imperfect. One possible explanation for this discrepancy is the effect of light refraction. In fact, projecting the visual stimulus onto a screen positioned outside the water tank, results in a distorted image from the perspective of an observer inside the water [40]. The stimulus appears compressed within a circular window corresponding to a cone with half-angle of $\approx 49^\circ$. In order to simulate the effect an external current one would like to reproduce an optic flow corresponding to a backward movement of the fish. Without refraction, and with a screen that covers most of the lower visual field, a forward translation of the pattern is equivalent to a backward translation of the fish. In the presence of refraction, however, the pattern inside the circular window still moves forward, while the window itself remains stationary relative to the fish, producing a conflicting stimulus. Many of the papers we discussed here seem to have ignored this problem, which could partly explain the lack of consistency among them. On the theoretical side, one would like to have a single interpretation that can describe most of the experimental observations reported in the literature. However, it is more common to find models tailored to reproduce the data presented within the same paper, often disregarding inconsistencies with earlier results. For example, Refs. [24,25] suggest that the fish modulate their response only based on the forward or external flow rates, but this is inconsistent with the ability of the fish to stabilize their position across different conditions, as shown in Refs. [21,22,38]. In Sec. IV, we address this conflict and propose a theoretical interpretation that accounts for most of the observations in zebrafish larvae. This interpretation is based on the mechanism that was proposed for visuomotor stabilization in danionella larvae [35], which we further develop in the following section.

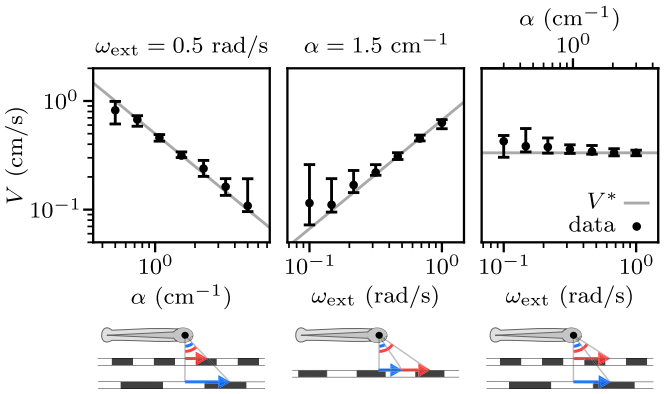

FIG. 2. End-of-trial swimming speed V in response to external currents for different values of feedback gain α and external flow rate ω_{ext}, from the experiments of Ref. [35]. The median swimming speed was calculated for each individual fish from the periods where it was swimming in response to the current in the last 10 s of the trials [black error bars, quartiles of the distributions across $N = (33, 31, 28)$ fish, from left to right]. The target speed is given by $V^* = \omega_{ext}/\alpha$ (gray lines). The schematics illustrate how parameter changes map to variations in pattern distance and current speed in the real world. The arrows indicate the current speed for two different parameter values (smaller in blue, larger in red).

III. STABILIZATION THROUGH CONTINUOUS LOCOMOTION

A. Experiments in danionella larvae

Here, we further analyze the results of Ref. [35], where visuomotor stabilization was investigated in danionella larvae. A head-restrained approach was used, with the visual pattern projected directly on the bottom of the tank, in order to avoid distortions due to light refraction. While zebrafish larvae move through a discrete series of swimming bouts, danionella larvae can swim continuously for minutes, resulting in a distinct behavioral response [34]. The fish were presented with external currents of 30 s duration for different values of external flow rate ω_{ext} and feedback gain α. Three different experiments were performed (Fig. 2, from left to right):

(1) Increasing α with constant ω_{ext}, corresponds to decreasing distance and current speed.

(2) Increasing ω_{ext} with constant α, corresponds to increasing current speed with constant distance.

(3) Increasing α and ω_{ext} proportionally, corresponds to decreasing distance with constant current speed.

The fish adapted their swimming speed V to approximately swim at the target speed $V^* = \omega_{ext}/\alpha$ for which the visual feedback compensates the external flow. It was shown that the observed adaptation results from a simple feedback control mechanism, combined with the fact that the nervous system encodes physical variables logarithmically. We now recapitulate how this mechanism works in the absence of noise, to make clearer the effect of each nonlinearity in the sensorimotor loop and how they shape the behavior of the system.

B. Delay-induced instability in linear feedback control

It was shown that there are significant delays in the sensorimotor loop underlying the optomotor response, such that a

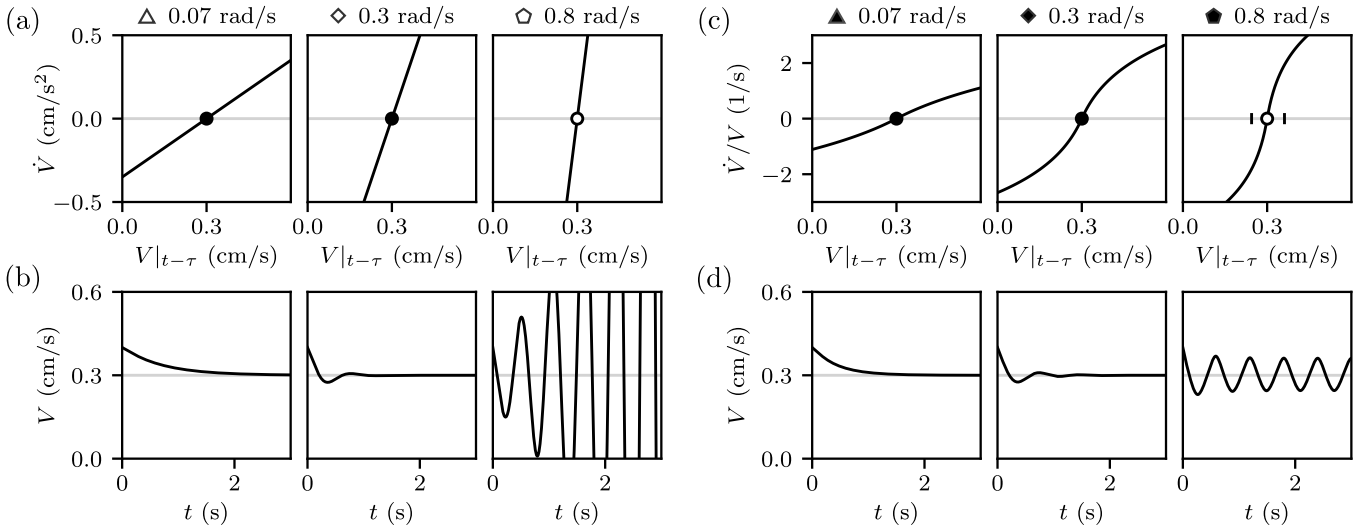

FIG. 3. Examples of response functions and swimming speed traces for the linear and nonlinear feedback control equations. (a) Linear response functions of Eq. (1) for three choices of ω_{ext} (values above the subplots) for a fixed target speed $V^* = 0.3$ cm/s. The black dots indicate stable fixed points and the white dot an unstable one. (b) Solutions of Eq. (1) for the corresponding parameters in panel (a) and an initial swimming speed $V_0 = 0.4$ cm/s. (c) Same as panel (a), but for the nonlinear response functions of Eq. (3). The black vertical lines indicate the amplitude of the limit cycle. (d) Same as panel (b), but for the solutions of Eq. (3). The symbols mark the corresponding points in the stability diagrams of Fig. 4. The parameter values here and in the following figures, unless otherwise stated, are $k = 5$ cm/s, $\tau = 0.15$ s, $r = 1.6\,\text{s}^{-1}$, and $\omega_c = 0.07$ rad/s.

change in optic flow rate at a given time only has an effect on the swimming speed after a delay $\tau \approx 150$ ms [23,35]. Following Ref. [35], we first consider the case of a linear system where the acceleration $\dot{V}$ to match the notation in Eq. (1) is proportional to the delayed net optic flow rate $\omega|_{t-\tau}$, with a responsiveness k:

$$\dot{V} = k\omega|_{t-\tau} = k(\omega_{\text{ext}} - \alpha V)|_{t-\tau}. \tag{1}$$

The solutions to this equation depend on the value of the dimensionless gain $\mu = k\alpha\tau$. They converge to the target speed $V^* = \omega_{\text{ext}}/\alpha$ exponentially for $\mu < 1/e$ and through damped oscillations for $1/e < \mu < \pi/2$, whereas they are diverging oscillations for $\mu > \pi/2$. Therefore the system becomes unstable if either responsiveness, feedback gain, or delay are increased above a critical value. To illustrate the behavior of the system we show the solutions for three different parameter values. We consider increasing values of the external flow rate ω_{ext} while keeping a constant target speed V^*. Therefore, the feedback gain α also increases proportionally to ω_{ext}. The increase in α leads to an increasing slope of the response function [Fig. 3(a)], eventually resulting in an unstable fixed point. The solutions showing the evolution of V over time [Fig. 3(b)] illustrate the three different dynamical regimes described above. As the characteristics of the external current are characterized by ω_{ext} and α we can summarize the behavior of the system in a two-dimensional stability diagram. Here, we equivalently chose one of the axes to be the target speed V^* [Fig. 4(a)]. We see that for any given V^*, the system becomes unstable as ω_{ext} is increased above a threshold $\pi V^*/(2k\tau)$, leading to diverging speed oscillations. It is important to note that this description must eventually break down, since the fish can only swim within a limited range of speed. Therefore, this model fails when V falls outside this range, as for example if it becomes negative.

Our analysis highlights that this feedback control model is problematic: for any given value of ω_{ext}, the system becomes unstable if the target speed V^* is too low. The fish cannot measure the value of V^* directly from sensory inputs, as it can with ω_{ext}. This is because V^* depends on α, which can only be estimated using efference copies of motor command to disentangle exafferent and reafferent visual inputs. In principle, this could be achieved by a forward internal model which would provide an internal estimate of the feedback gain α. Using this information, the fish could then adapt its responsiveness k to

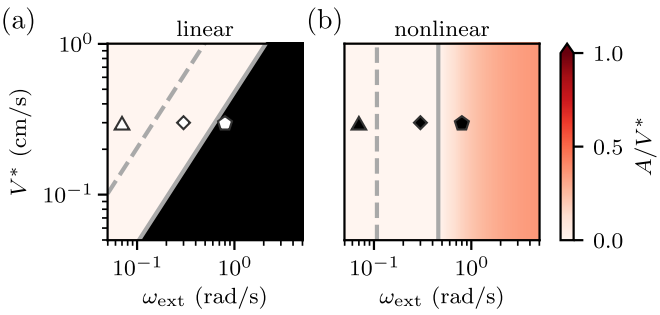

FIG. 4. Stability diagrams for the linear and nonlinear feedback control equations. Amplitude A of the steady-state solution for (a) Eq. (1) and (b) Eq. (3), for different values of the target speed V^* and the external flow rate ω_{ext}. The region where the system is unstable is colored in black. The limit cycle amplitude was computed according to the approximation described in the text. The gray dashed lines indicate the transition to oscillatory behavior, whereas the solid ones indicate the bifurcation boundary.

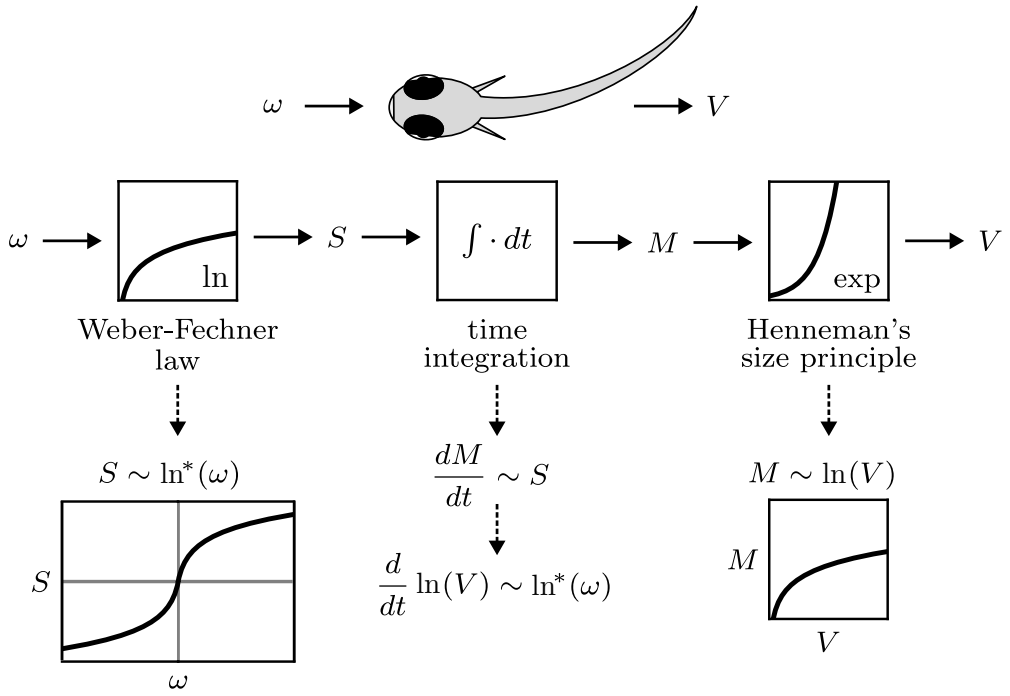

FIG. 5. Sensorimotor transformations underlying visuomotor stabilization. The optic flow rate ω is logarithmically compressed at the sensory end, producing a sensory drive S. This signal is integrated over time to generate a motor drive M, which is exponentially expanded at the motor end, resulting in the swimming speed V.

reach the target quickly while also avoiding instability. However, in Ref. [35], it was shown that a different mechanism actually prevents this instability and gives rise to adaptive responsiveness without motor learning.

C. Effect of logarithmic transformations

The behavior of the system was found to arise from the presence of nonlinear sensorimotor transformations that were not included in Eq. (1) (Fig. 5). It was shown that both the optic flow rate and the swimming speed are encoded logarithmically in the brain, in accordance with the Weber-Fechner law and Henneman's size principle, respectively [36,37]. This results in a logarithmic compression from the optic flow rate ω to a corresponding sensory drive S and an exponential expansion from a motor drive M to the corresponding swimming speed V. Finally, the motor drive is taken to be proportional to the integral of the sensory drive through a rate coefficient r, yielding the three following sensorimotor transformations:

$$S = \ln^*(\omega/\omega_c), \tag{2a}$$

$$\dot{M} = rS, \tag{2b}$$

$$V = V_c e^M, \tag{2c}$$

where the parameters ω_c and V_c specify the transformation from optic flow rate to sensory drive and from motor drive to swimming speed, respectively. For the sensory drive, we considered a shifted logarithm of the form $\ln^*(x) = \mathrm{sgn}(x)\ln(1 + |x|)$, which is continuously differentiable close to the origin to make the system easier to study analytically. We actually expect the fish to be unable to detect flow rates with a magnitude falling below a certain threshold ω_{th}, and a more accurate transformation would be a thresholded logarithm of the form $\ln_{th}(x) = \mathrm{sgn}(x)\ln(|x|)H(|x| - 1)$, with H being the Heaviside step function. Both functional forms lead to analogous conclusions, differing only in their behavior for small flow rates comparable with the detection threshold.

Combining Eq. (2) and including the time delay τ, we obtain the following equation for the dynamics of V:

$$\dot{V}/V = r\ln^*(\omega/\omega_c)|_{t-\tau}. \tag{3}$$

In Ref. [35], the response function of the fish was estimated, yielding the values $r \approx 1.6\,\mathrm{s}^{-1}$ and $\omega_c \approx 0.07$ rad/s, which we consider here. While Ref. [35] included a multiplicative noise term in Eq. (3) to reproduce the experimentally observed speed traces, here we consider only the deterministic part of the dynamics to examine the effect of the nonlinearities on the response of the system. We can still linearize Eq. (3) to study the dynamics close to the target speed V^*, recovering a linear equation of the form of Eq. (1), with the dimensionless gain now given by $\mu_0 = r\tau\omega_{ext}/\omega_c$. For $\mu_0 < \pi/2$, the fixed point is stable and the solutions converge to it as in the linear case. For $\mu_0 > \pi/2$, the presence of the nonlinearities prevents the system from diverging and the solutions converge to a stable limit cycle, corresponding to regular speed oscillations around the target speed. In the limit of small oscillations it was shown that the amplitude of the swimming speed oscillations grows linearly with the bifurcation parameter as $A \simeq 1.7(\omega_c/\alpha)(\mu_0 - \pi/2)$. Thus, the relative oscillation amplitude A/V^* remains bounded as ω_{ext} increases. We plotted the stability diagram as for the linear system, finding that the stability of the system now depends only on the external

flow rate ω_{ext} [Fig. 4(b)]. At $\mu_0 = \pi/2$, one observes a Hopf bifurcation, followed by limit cycle oscillations with a finite amplitude. This result holds close to the bifurcation, but as the system is driven further away from it A/V^* is expected to grow logarithmically with ω_{ext}, and eventually break the limit of small oscillations. On the other hand, we also expect the response to eventually saturate for large enough ω_{ext}, similarly to how we expect it to vanish below a certain detection threshold. Such saturation could be incorporated into the functional form of the sensory drive S, limiting the growth of the relative oscillation amplitude and resulting in confined oscillations around the target speed even for very large values of ω_{ext}. As in the linear case, we plotted the solutions for three increasing values of ω_{ext} corresponding to different dynamical regimes [Fig. 3(d)]. The slope of the response function at the fixed point still increases with ω_{ext}, resulting in an unstable fixed point, but now the sublinear response results in limit cycle oscillations [Fig. 3(c)].

We can now clearly distinguish the effects of the two nonlinear transformations. The logarithmic compression at the sensory end limits the responsiveness as the swimming speed deviates from the target in such a way that the relative amplitude of the oscillations around it remains bounded. On the other hand, the exponential expansion at the motor end results in a responsiveness that is proportional to the swimming speed itself, so that the dependence on the feedback gain is replaced by a dependence on the external flow rate. This is advantageous because, unlike α, ω_{ext} can be directly measured from visual inputs. Given that the fish can only detect a limited range of optic flow rates, the response magnitude r can be set, for example through natural selection, so that the responsiveness remains sufficiently high across this entire range.

D. Initiation of swimming

Reference [35] only considered how the fish continuously adapt their swimming speed to stabilize their position, not how swimming is initiated in response to the appearance of a visual flow. Here, we further analyze the same data to gain insight into this process. The termination of swimming could be included in the model by assuming that the fish stop swimming soon after their speed V reaches the boundaries of the range of physiologically accessible speeds $[V_{min}, V_{max}]$. In this way one can reproduce the observations that fish stop swimming after their speed reaches a maximum V_{max} in open-loop conditions, or after it reaches a minimum V_{min} after the external current is removed [35].

For the same experiments described in Sec. III A, we extracted the initial speeds V_0 as the maximum speed reached by the animal in the first time τ after initiation of swimming [Fig. 6(a)] and the reaction times T_r between the appearance of the external current and the moment when the fish start swimming [Fig. 6(b)].

The initial speed V_0 seems largely independent of α and ω_{ext}, remaining close to the upper bound of the physiological speed range. Although we observe a slight increasing trend with ω_{ext}, the fish generally seem to always start swimming at high speeds.

The reaction time is independent of α and decreases with ω_{ext}. Its independence from α is expected, as the fish cannot know the feedback gain before starting to swim. Interestingly, the width of the T_r distribution grows proportionally with T_r itself, resulting in uniform widths when plotted on a logarithmic scale. To clarify this, we plotted histograms of the logarithm of the measured values of T_r for different values of ω_{ext} (Fig. 7). The distributions are peaked and approximately Gaussian, suggesting that the reaction times follow lognormal distributions.

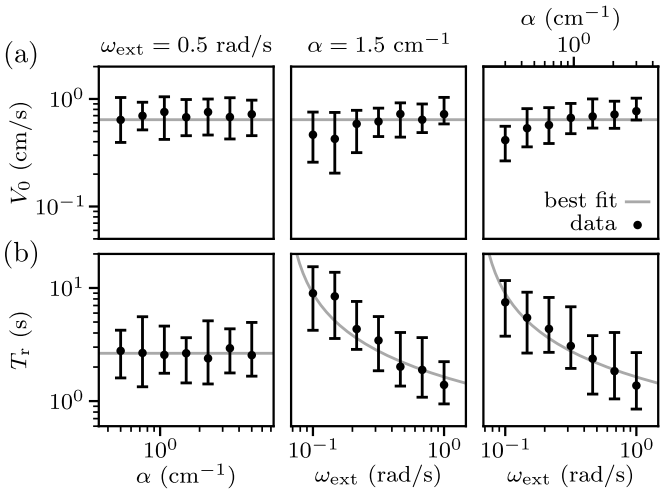

FIG. 6. Initial speeds V_0 (a) and reaction times T_r (b) in response to external currents for different values of feedback gain α and external flow rate ω_{ext}, from the same experiments as in Fig. 2. Error bars denote the quartiles of the distributions [data from $N = (33, 31, 28)$ fish, from left to right]. The initial speed was estimated as the maximum swimming speed attained in the first 150 ms following initiation of swimming. Trials in which fish were already swimming at the onset, or never started swimming, were excluded from the distributions. T_r as function of ω_{ext} is well fitted by a reciprocal logarithmic dependence [Eq. (4)], whereas all other plots are well fitted by a constant (gray lines).

Reference [39] proposed that larval zebrafish initiate swimming stochastically via a Poisson process, which would produce exponential distributions of reaction times. In contrast, we observe unimodal distributions with a positive peak, suggesting that swimming initiation involves an integration process. We can consider a simple deterministic accumulation model in which the sensory drive S is integrated over time, and the fish initiates swimming when the integrated signal $\Phi = \int S(t)dt$ reaches a threshold Φ_r. This kind of model has been proposed as a fundamental mechanism underlying decision making and reaction time processes [41]. For a constant ω_{ext}, it would result in a reaction time $T_r = \Phi_r/S(\omega_{ext})$.

The dependence of reaction times on stimulus intensity has been traditionally fitted with decreasing power laws, and interpreted either as reflecting nonlinear transformations of the stimulus or resulting from the integration mechanism itself [42]. In our simple accumulation model, T_r decreases with ω_{ext} with a dependence that is determined by the nonlinear compression of the sensory drive S. Here, we can consider the thresholded logarithm $\ln_{th}$ as the optic flow rate remains positive before swimming is initiated, resulting in a reciprocal

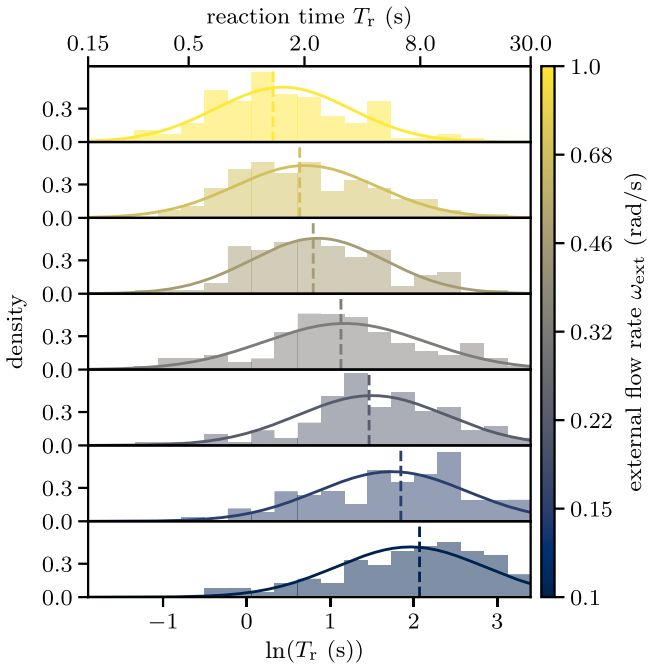

FIG. 7. Distribution of reaction times for different values of the external flow rate. Each subplot shows the histogram of the logarithm of the reaction time T_r, pooling the measurements shown in Fig. 6(b) for the same value of ω_{ext} (corresponding color bar). The distributions are well fitted by Gaussian distributions of comparable widths (solid lines). The medians of the distributions decrease with ω_{ext} (vertical dashed lines).

logarithmic dependence for the reaction times:

$$T_r = \frac{\Phi_r}{\ln(\omega_{ext}/\omega_{th})}, \quad \text{for } \omega_{ext} > \omega_{th}. \tag{4}$$

We fitted the observed dependence with this functional form and found that it fits well the data with $\Phi_r \approx 5$ s and $\omega_{th} \approx 0.03$ rad/s [Fig. 6(b)]. In fact, the estimated value of ω_{th} is consistent with the one estimated in Ref. [35] by directly measuring the response function.

If we admit that the motor drive M starts increasing due to the presence of the external flow before initiation of swimming, then Eq. (2) predicts that the fish would start swimming at a speed $V_c e^{\Phi_r}$, independent of ω_{ext} and α. This is also consistent with our observation that the initial speed V_0 is approximately constant [Fig. 6(a)].

To understand the observed variability in reaction times for any given value of ω_{ext} (Fig. 7), we hypothesize that it arises from a variability in the internal sensory drive S. Rather than being constant, S is assumed to fluctuate due to a source of multiplicative noise, such that its coefficient of variation remains constant. Then, its values will follow a lognormal distribution $S \sim \text{Lognormal}(\ln(m_S), \sigma_r^2)$, where m_S is the median of S and σ_r controls the relative magnitude of the fluctuations. This assumption seems reasonable, as neuronal firing rates, along with many other structural and functional properties of the brain, have been shown to follow lognormal statistics [43].

If S is lognormally distributed, then the resulting reaction time $T_r = \Phi_r/S(\omega_{ext})$ will also follow a lognormal distribution $T_r \sim \text{Lognormal}(\ln(\Phi_r/m_S), \sigma_r^2)$. The observed fluctuations of T_r are compatible with the described mechanism, as for different ω_{ext} we find that a lognormal distribution provides a good fit, with approximately the same value of $\sigma_r \approx 0.9$ (Fig. 7). In fact, experimentally measured reaction times in other contexts have been successfully fitted with the lognormal distribution, and other possible explanations for how this distribution arises have been proposed [44].

E. Drift correction

We have seen the fish start swimming at a speed V_0 close to the maximum attainable speed V_{max}. Then, following Eq. (3) for the evolution of the speed would result in V approaching the target V^* with a rate of the order of $r\omega_{ext}/\omega_c$. Using the estimated values of r and ω_c, we would therefore expect V to approach V^* on a subsecond timescale in our experiments. However, this is not what is observed. Looking at the transient evolution of V after initiation of swimming, one finds a slow convergence occurring over several seconds [Figs. 8(a)–8(c)]. This becomes particularly clear when plotting the estimated sensory drive and observing how it gradually approaches zero [Figs. 8(d)–8(f)].

If the goal of this behavioral reflex is to maintain the position of the fish stationary, this observation can be understood as follows. Before initiation of swimming, the fish perceives a sustained forward flow rate for a time T_r, corresponding to a backward drift of its position by a distance $\omega_{ext} T_r/\alpha$. To correct for this backward drift, the fish must temporarily swim faster than the target speed in order to restore its position to the value prior to the appearance of the current. While Eq. (2) does not account for this phenomenon, we can propose a simple mechanism that does. We can introduce a second term that contributes to the evolution of the motor drive M while the fish is swimming. This correction term can simply be proportional to the accumulated sensory drive Φ, leading to the following equation:

$$\dot{M} = rS + r\lambda_c \Phi, \tag{5}$$

where the rate λ_c determines the magnitude of the correction. This way, any kind of positional drift leads to an accumulation of Φ, which drives the motor drive to compensate for the drift while simultaneously driving Φ back to zero. The advantage of this mechanism is that it not only corrects for the drift accumulated before swimming initiation, but also compensates for other possible sources of drift, such as asymmetries in the response function, which have been observed experimentally in some fish [35].

If λ_c is small compared to the convergence rate of Eq. (3), Eq. (5) can be approximately solved using a separation of timescales. Over short timescales, we consider the second term in Eq. (5) to be effectively constant, while the dynamics of the first term lead to a quasi-steady-state. Considering $\dot{M} = 0$, we find the quasi-steady-state sensory drive $S_{qss} = -\lambda_c \Phi$. Therefore, V will not converge toward V^*, but rather toward the quasi-steady-state fixed point:

$$V_{qss} = V^* + \text{sgn}(\Phi)\frac{\omega_c}{\alpha}(e^{\lambda_c|\Phi|} - 1). \tag{6}$$

If the accumulated sensory drive is positive $\Phi > 0$, then V converges to a value larger than V^* in order to compensate

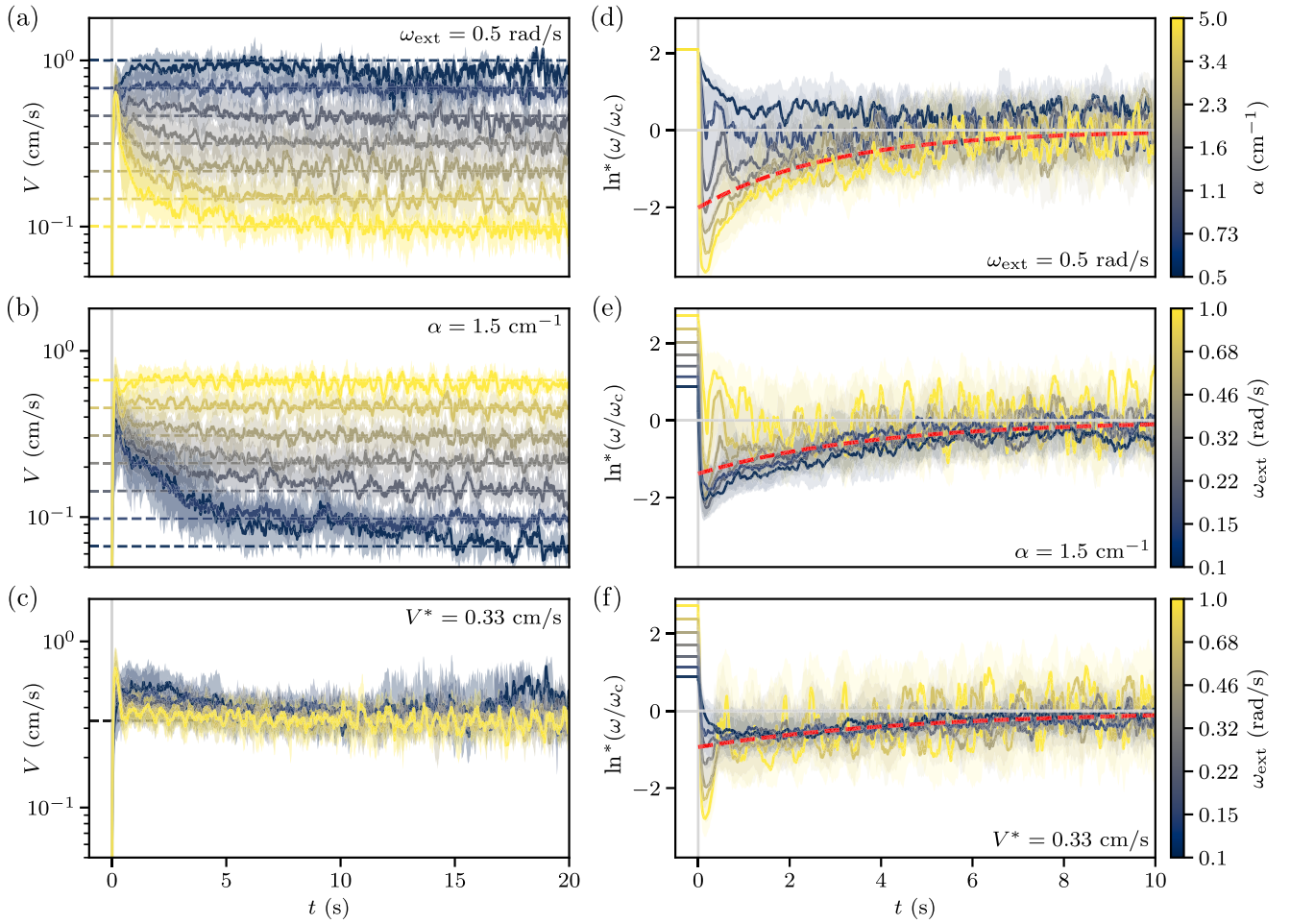

FIG. 8. Initial speed transients in response to external currents for different values of feedback gain α and external flow rate ω_{ext}, from the same experiments as in Fig. 2. (a) Traces of swimming speed V over time, aligned such that the initiation of swimming corresponds to $t = 0$, for the experiments with different values of α (color-coded values) with a constant ω_{ext}. The swimming speed (solid lines and shaded areas indicate the quartiles of the distributions) converge to the corresponding target speeds (dashed lines). (b) Same as panel (a), but for the experiments with different values of ω_{ext} with a constant α. (c) Same as panel (a), but for experiments with different values of α and ω_{ext} such that their ratio is fixed. (d) Traces of sensory drive $S = \ln^*(\omega/\omega_c)$ estimated from the speed transients of panel (a). The sensory drive (solid lines and shaded areas indicate the quartiles of the distributions) converges to zero approximately following an exponential decay (red dashed line, best fit). (e) Same as panel (d), but estimated from the speed transients of panel (b). (f) Same as panel (d), but estimated from the speed transients of panel (c).

for the accumulated drift. Conversely, if $\Phi < 0$, meaning that the fish has been swimming faster than the current, then $V_{qss} < V^*$. Thus, over short timescales, V either converges toward V_{qss} or oscillates around it in a delay-induced limit cycle. To determine how this quasi-steady-state evolves over longer timescales, we consider the defining equation for the accumulated sensory drive $\dot{\Phi} = S$, and substitute our result for S_{qss}, finding $\dot{S}_{qss} = -\lambda_c S_{qss}$. We therefore find that the quasi-steady-state sensory drive decays exponentially to zero with a rate λ_c.

Before swimming begins, Φ accumulates a positive sensory drive up to a typical value of Φ_r (see Sec. III D), corresponding to a negative quasi-steady-state sensory drive at initiation $S_{qss}(0) = -\lambda_c \Phi_r$, and therefore $V_{qss}(0) > V^*$. Afterward, we expect the sensory drive to decay exponentially as $S_{qss}(t) = -\lambda_c \Phi_r e^{-\lambda_c t}$. Indeed, we find that, after a quick transient following swimming initiation, the traces of S for most of the parameter values converge to a similar value, which then slowly approaches zero [Figs. 8(d)–8(f)]. This behavior is not observed for parameter values where the target speed V^* is close to V_{max}, as the fish cannot attain speeds significantly higher than the target. Excluding the experiments for which $V^* > 0.6$ cm/s, we fitted the average sensory drive following swimming initiation with exponential decays. We found similar best-fit values of $\Phi_r \approx 5$ s and $\lambda_c \approx 0.27\,\text{s}^{-1}$ for the three different experimental protocols. The value of Φ_r agrees with the one obtained in Sec. III D when analyzing reaction times, while the value of λ_c provides a posteriori confirmation of the validity of our timescale separation hypothesis.

For simplicity, we have assumed a perfect integration Φ of the sensory drive S, but it could be reasonable to include a leak term, resulting in a leaky integration over a timescale of several seconds. This modification does not change the analysis qualitatively, but only slightly increases the decay rate of the quasi–steady-state solution.

IV. STABILIZATION THROUGH INTERMITTENT LOCOMOTION

A. Intermittent swimming in zebrafish

Here, we extend the framework that we developed for continuous locomotion in the previous section to the case of intermittent locomotion. Because of the universality of the principles underlying the nonlinear sensorimotor transformations illustrated in Fig. 5, we expect a similar control process to remain valid in the case of intermittent swimming. In this way, the same mechanism could underlie adaptive stabilization as danionella grow larger and transition to intermittent swimming [45], as well as in other species such as zebrafish. In fact, we will show that this framework can explain the experimental observations of visuomotor stabilization in the larval zebrafish (see Sec. II B). In this case, we hypothesize that the control process functions similarly to the case of continuous swimming (Fig. 5), in which the optic flow is first compressed and then integrated in time, accumulating into a motor drive M. The key difference is that, while in the continuous case M is directly reflected in the swimming speed V, in the intermittent case, M regulates the swimming speed V only at the times when the animal swims.

In freely swimming conditions, the swimming bouts of zebrafish exhibit a stereotyped speed profile, characterized by an initial peak lasting approximately ≈200 ms, followed by a decay to zero [24]. Upon normalizing each profile by its average speed V_b, all traces collapse onto the same curve.

Thus, if the bout duration T_b is defined using a speed threshold, one finds that T_b increases with the bout speed V_b, regardless of whether the threshold is applied to the speed of the fish or of its tail movements [24,38]. Because of the peaked shape of the speed profile the bout duration is not strongly modulated with bout speed, remaining of the order of $T_\mathrm{b} \approx 200$ ms, which we take as the nominal bout duration in the following. This observation suggests that the observed variations in T_b arise from corresponding variations in V_b. Since the relative variations of T_b remain small compared to those of V_b we focus on the dynamics of the speed and assume a constant bout duration for simplicity.

It was shown in head-restrained experiments that the fish can adjust the speed of the tail mid-bout in response to perturbations of the visual feedback [23], but this modulation only takes place in the final part of the bout, therefore we do not expect it to significantly affect the speed of the fish. Here, we do not go into the details of how such a speed profile arises. Instead, we assume that a mechanism exists that terminates swimming shortly after it started, resulting in discrete swimming events. Nevertheless, it is worth noting that sensorimotor delays involved in the control of swimming speed have been proposed to play a role in determining such speed profiles and the termination of swimming underlying intermittent locomotion [45].

For simplicity, we consider the swimming speed to have a constant value V_b for the duration T_b of a bout (Fig. 9). Then, for an external current with a constant flow rate ω_ext, the motor drive M will increase at a constant rate in the absence of visual feedback. When the fish swims, the net optic flow rate becomes $\omega_\mathrm{ext} - \alpha V_\mathrm{b}$, decreasing the rate of change of M, which becomes negative for a backward optic flow. When the fish initiates a bout, the swimming speed V_b is determined by the value of the motor drive M at that instant.

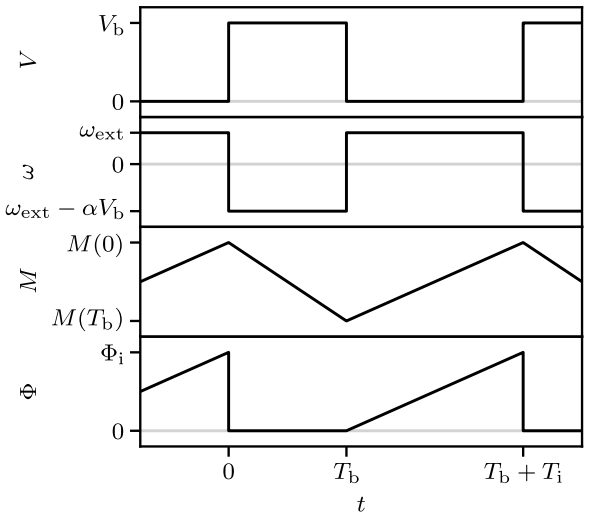

FIG. 9. Schematic that illustrates the time-dependent variables in a simplified model of intermittent swimming. The swimming speed V changes between 0 when the fish is not swimming for the duration T_i of the interbout interval to the bout speed V_b for the duration T_b of the bout. The motor drive M grows when the net optic flow rate ω is positive because of the external current and decreases when ω is negative because of the contribution of visual feedback. During the interbout interval, the accumulated sensory drive Φ increases linearly up to a threshold Φ_i.

We do not consider the effect of sensorimotor delays in this case, as they do not significantly change the behavior of the system. Upon bout initiation, a short delay occurs before the tail movements affect the perceived optic flow and, consequently, the update of the motor drive. As a result, M continues to increase for a duration τ following the release of the motor command, after which the perceived visual feedback drives a different evolution for a duration T_b. Thus, the sensorimotor delay only affects the interbout dynamics by introducing a refractory period during which the fish still perceives a delayed backward optic flow, even if it has already stopped swimming.

Now, if the fish swims at speed V_n at the nth bout, then we can simply compute the variation of M due to the net optic flow until the following bout and express the speed of the following bout in terms of that of the previous one $V_{n+1} = f(V_n)$. This gives us a discrete dynamical system for the evolution of the bout speed V_b. We will investigate the behavior of the system for different forms of the function f, corresponding to either linear or nonlinear sensorimotor transformations. First, we look at the dynamics of bout initiation, which determine the interbout duration T_i.

B. Interbout duration in zebrafish

In freely swimming experiments where the feedback gain α was manipulated by changing the distance of the visual pattern, it was shown that the rate of swimming bouts f_b depends on the external flow rate ω_ext, but not on α [24]. This suggests that the mechanism for bout initiation is independent

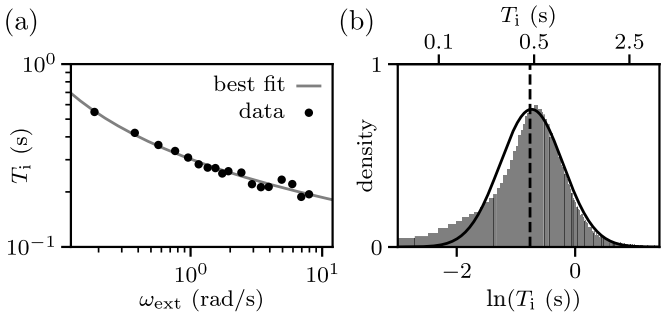

FIG. 10. Interbout duration in larval zebrafish. (a) Interbout duration T_i in freely swimming larval zebrafish as a function of the flow rate ω_{ext} of an external visual current (black points). The data are well fitted by a reciprocal logarithmic dependence [gray line; see Eq. (4)]. Data from Ref. [38]. (b) Histogram of the logarithm of the interbout durations T_i in freely swimming larval zebrafish in the absence of external visual currents. The dashed line indicates the median while the solid line is a Gaussian distribution which fits the data. Data from Ref. [46].

of the intensity of visual feedback. While the bout speed V_b is governed by the motor drive M, whose value depends on both ω_{ext} and α, the interbout duration T_i should only depend on ω_{ext}.

Other experiments in restrained conditions have shown that f_b can also be modulated by changing α [21,23]. This effect could be explained by the fact that restraining the fish alters the observed response [38]. Here, we will follow the observations in freely swimming conditions and consider a mechanism for bout initiation that depends solely on ω_{ext}.

We consider the simple accumulation model previously used for the initiation of swimming in danionella (Sec. III D). Here, we assume that the accumulated sensory drive Φ resets to zero after each swimming bout, such that it only depends on the forward optic flow experienced during the interbout interval. Analogous to Eq. (4), the interbout duration is then given by $T_i = \Phi_i / \ln(\omega_{ext}/\omega_{th})$ for $\omega_{ext} > \omega_{th}$, where Φ_i is the threshold for bout initiation (Fig. 9). Following the same reasoning as in Sec. III D, fluctuations in the sensory drive would lead to a lognormal distribution for T_i.

We used the functional form predicted by the model to fit the dependence of the interbout duration on the external flow rate from experiments on freely swimming zebrafish [38] [Fig. 10(a)]. The reciprocal logarithm provides a good fit to the data, with best-fit parameters $\Phi_i \approx 1.1$ s and $\omega_{th} \approx 0.03$ rad/s. The estimated value of ω_{th} is consistent with the one obtained for danionella in Sec. III D.

We can even extend the model to spontaneous navigation in the absence of external currents, where larval zebrafish initiate swimming bouts with a variable interbout duration T_i. The distribution of interbout durations is unimodal with a peak at ≈500 ms [46]. Experimentally measured histograms of T_i have been fitted with a negative binomial distribution. Although this fit captures the data, the negative binomial is intended to model a discrete random variable, whereas the interbout duration is continuous. Moreover, it provides no insight into the possible mechanisms underlying swimming initiation. We found that the same histogram can be fitted equally well by a lognormal distribution, which is consistent with our hypothesized mechanism for swimming initiation [Fig. 10(b)]. After a swimming bout terminates, an internal drive is integrated over time until it reaches a threshold sufficient to trigger the next bout. In the absence of salient external stimuli, we expect this internal drive to remain approximately constant, although it may be modulated over long timescales by external factors, such as temperature [47], or internal ones, such as hunger [48].

C. Feedback control with linear transformations

Before examining the effects of the nonlinear transformations studied in the context of continuous locomotion (Fig. 5), we first analyze the behavior of the system in the absence of nonlinearities. We consider $\dot{M} = k\omega$, so that the motor drive M is simply proportional to the integral of the optic flow rate ω with responsiveness k, while the bout speed $V_n = M(t_n)$ directly reflects the motor drive at the time of the bout. As the fish swims with speed V_n at time t_n, the motor drive changes first with rate $k(\omega_{ext} - \alpha V_n)$ for the duration of the visual feedback T_b and then with rate $k\omega_{ext}$ for the duration of the interbout interval T_i. We can then express the swimming speed of the following bout as

$$V_{n+1} = V_n + k(\omega_{ext} - \alpha V_n)T_b + k\omega_{ext}T_i. \tag{7}$$

The fixed point of this linear difference equation can be found by setting $V_{n+1} = V_n$, finding

$$V^*_{lin} = \frac{\omega_{ext}}{\alpha}\left(1 + \frac{T_i}{T_b}\right). \tag{8}$$

This is the speed at which the feedback flow rate exactly compensates the external flow rate over the interval between two consecutive bouts, corresponding to a fish that, on average, maintains a stable position. The solution to Eq. (7) can be written explicitly in terms of the initial condition V_0 and the fixed point V^*_{lin} using the geometric sum formula [49]:

$$V_n = (V_0 - V^*_{lin})(1 - k\alpha T_b)^n + V^*_{lin}. \tag{9}$$

Equation (9) holds for $k\alpha T_b \neq 0$, otherwise V simply grows by the same amount $k\omega_{ext}(T_b + T_i)$ at each step. We see that the behavior of the solution depends on the dimensionless parameter combination $k\alpha T_b$. For $0 < k\alpha T_b < 1$, the speed converges exponentially to V^*_{lin}. For $1 < k\alpha T_b < 2$, the speed also converges to V^*_{lin}, but alternates above and below it at each step. For $k\alpha T_b > 2$, the fixed point becomes unstable and the speed diverges, again alternating above and below V^*_{lin} at each step.

To illustrate these three distinct dynamical regimes, we plot the solutions for three different values of $k\alpha T_b$ (Fig. 11). These solutions can also be constructed graphically as cobweb plots, by plotting V_{n+1} as a function of V_n and iterating the map by moving vertically from the identity line to this curve and horizontally back to the identity line to obtain successive bout speeds.

The parameter combination $k\alpha T_b$, which controls the system behavior, can be interpreted as the relative change in speed in the next bout caused by the visual feedback resulting from the current bout. If $k\alpha T_b > 1$ we see that the system overcorrects and overshoots the target at each step, if $k\alpha T_b >$

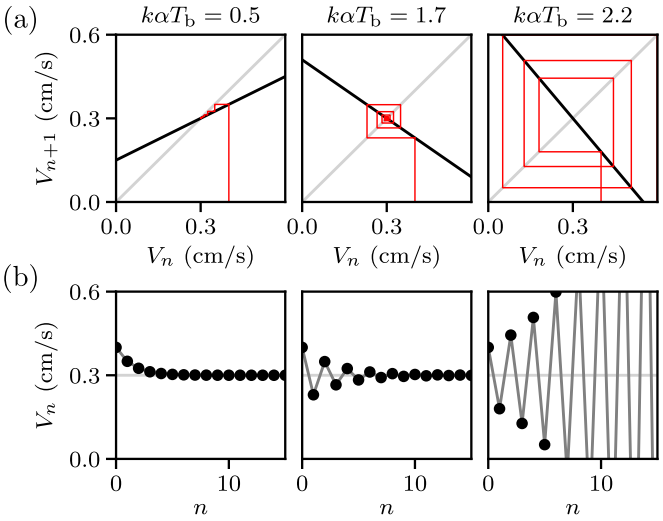

FIG. 11. Examples of cobweb plots and swimming speed sequences for the linear difference equation. (a) Iterated maps (black lines) from Eq. (7) and corresponding cobweb constructions (red lines) for three different values of the parameter combination $k\alpha T_b$, with initial condition $V_0 = 0.4$ cm/s and target speed $V^*_{\text{lin}} = 0.3$ cm/s. (b) Solutions of Eq. (7) corresponding to the cobweb construction in panel (a).

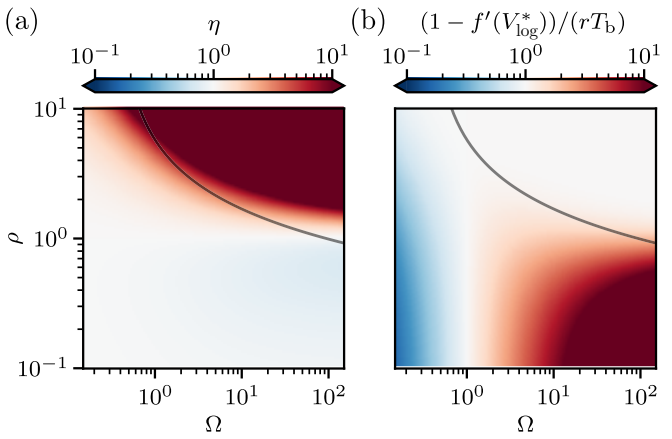

FIG. 12. Parameter dependence of the fixed point of the nonlinear map [Eq. (11)]. (a) Ratio η between the fixed point of the nonlinear map and that of the linear one, as a function of the dimensionless parameter ratios $\rho = T_i/T_b$ and $\Omega = \omega_{\text{ext}}/\omega_c$ [Eq. (13)]. The relationship between T_i and ω_{ext} from the best fit of Fig. 10(b) is plotted as a solid line. (b) Deviation from the identity of the slope $f'(V^*_{\log})$ of the nonlinear map at the fixed point as a function of ρ and Ω [Eq. (15)].

2 these overcorrections grow in size at each step, making the system unstable. This instability is analogous to the one discussed in the case of continuous locomotion (Sec. III B). The difference is that, in that case, the instability was due to the presence of sensorimotor delays, whereas here it results from the fact that the fish can only control its speed at discrete times, due to the intrinsically intermittent nature of its locomotion. The system becomes unstable if either the responsiveness k or the feedback gain α become sufficiently large. While the parameter k is intrinsic to the fish, α depends on the specific environment surrounding the fish, indicating that the same problem observed in Sec. III B also occurs in the case of intermittent locomotion. We now examine how this behavior changes when logarithmic transformations are taken into account, in analogy with the analysis of Sec. III C.

D. Feedback control with logarithmic transformations

We have seen that logarithmic transformations prevent dynamical instabilities in the case of continuous locomotion. Here, we investigate their effect on visuomotor stabilization during intermittent locomotion. We consider the same sensorimotor transformations as in Eq. (2), and derive a difference equation for the speed of a swimming bout in terms of that of the previous one, analogous to the linear case. Now, the motor drive changes with rate $r \ln^*((\omega_{\text{ext}} - \alpha V_n)/\omega_c)$ for a time T_b and with rate $r \ln^*(\omega_{\text{ext}}/\omega_c)$ for a time T_i, resulting in the following nonlinear difference equation for the swimming speed:

$$\ln\left(\frac{V_{n+1}}{V_n}\right) = rT_b \ln^*\left(\frac{\omega_{\text{ext}} - \alpha V_n}{\omega_c}\right) + rT_i \ln^*\left(\frac{\omega_{\text{ext}}}{\omega_c}\right). \quad (10)$$

Equation (10) can be further simplified using the fact that $\exp(\ln^*(x)) = (1 + |x|)^{\text{sgn}(x)}$, leading to

$$V_{n+1} = V_n\left(1 + \frac{|\omega_{\text{ext}} - \alpha V_n|}{\omega_c}\right)^{\sigma r T_b}\left(1 + \frac{\omega_{\text{ext}}}{\omega_c}\right)^{rT_i}, \quad (11)$$

where we defined $\sigma = \text{sgn}(\omega_{\text{ext}} - \alpha V_n)$. To stabilize its position, the fish must swim at a speed V_n larger than $\omega_{\text{ext}}/\alpha$, corresponding to a backward net optic flow during the bout and $\sigma = -1$.

Equation (11) has a trivial fixed point $V^*_0 = 0$, corresponding to the absence of swimming, and another one corresponding to a finite value of the speed $V^*_{\log} > \omega_{\text{ext}}/\alpha$:

$$V^*_{\log} = \frac{\omega_c}{\alpha}\left[\left(1 + \frac{\omega_{\text{ext}}}{\omega_c}\right)^{\frac{T_i}{T_b}} - 1 + \frac{\omega_{\text{ext}}}{\omega_c}\right]. \quad (12)$$

We note that this expression differs from the one corresponding to an exact stabilization of the position [Eq. (8)], which we obtained as the fixed point V^*_{lin} of the linear difference equation [Eq. (7)]. This difference is expected as in the nonlinear case the fish does not adjust its speed to maintain the optic flow rate ω constant on average, but rather its logarithmic representation S. The two solutions coincide only for $T_i = T_b$, in which case the optic flow rates during swimming and resting periods are opposite, yielding $V^*_{\log} = V^*_{\text{lin}} = 2\omega_{\text{ext}}/\alpha$.

To quantify the discrepancy between $V^*_{\log}$ and V^*_{lin}, we can study their ratio η [Fig. 12(a)]:

$$\eta = \frac{V^*_{\log}}{V^*_{\text{lin}}} = \frac{1 + \frac{1}{\Omega}[(1 + \Omega)^\rho - 1]}{1 + \rho}, \quad (13)$$

which only depends on the ratios $\Omega = \omega_{\text{ext}}/\omega_c$ and $\rho = T_i/T_b$. We see that $\eta > 1$ for $\rho > 1$, with the fish swimming faster than the target and moving forward on average, whereas $\eta < 1$ for $\rho < 1$, with the fish moving slower and drifting backward. We find that $\eta = 1$ when $\rho = 1$, meaning that the

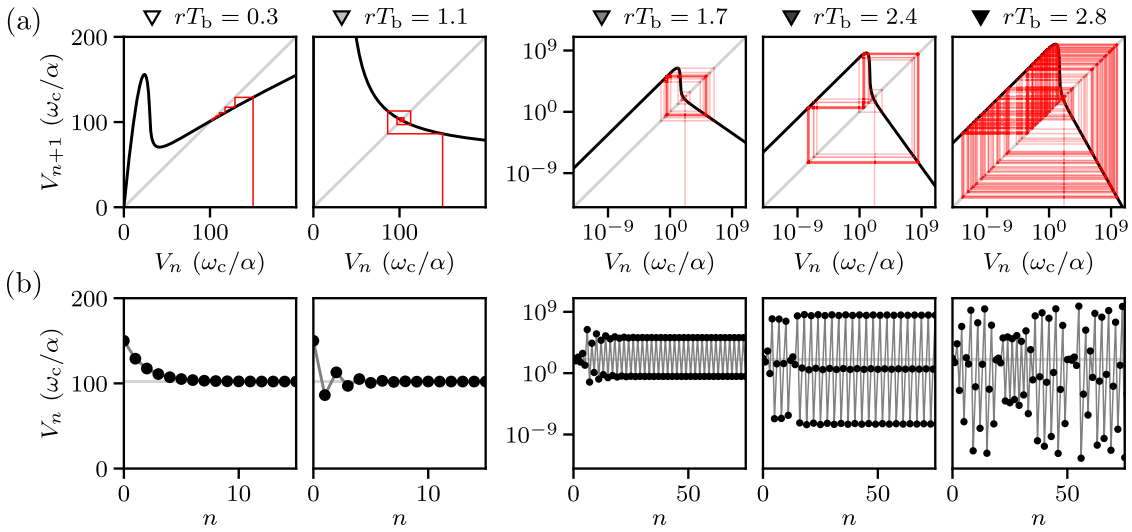

FIG. 13. Examples of cobweb plots and swimming speed sequences for the nonlinear difference equation. (a) Iterated maps (black lines) from Eq. (11) and corresponding cobweb constructions (red lines) for five different values of the parameter combination rT_b, with initial condition $V_0 = 150\omega_c/\alpha$, for $\Omega = 30$ and $\rho = 1.25$. (b) Solutions of Eq. (11) corresponding to the cobweb construction in panel (a). The triangles mark the corresponding values in the bifurcation diagram of Fig. 14.

fish stabilizes its position exactly when $T_i = T_b$. In the limit $\Omega \to 0$, $\eta \to 1$ independently of ρ. In the limit $\Omega \to \infty$, $\eta \to 1/(1+\rho)$ for $\rho < 1$, whereas $\eta \to \infty$ for $\rho > 1$.

Intuitively, the fish tends to swim at a speed that balances the logarithms of forward and backward optic flow rates, weighted by their corresponding durations. For large Ω, we can approximately write $T_b \ln(\alpha V^*_{\log} - \omega_{ext}) \sim T_i \ln(\omega_{ext})$, which leads to the scaling $V^*_{\log} \sim (\omega_{ext} + \omega^{\rho}_{ext})/\alpha$, consistent with Eq. (12).

Because of its nonlinear nature, we cannot explicitly solve Eq. (11) as we did for Eq. (7). Nevertheless, we can study the stability of its fixed points to understand its behavior. To do so, we can linearize the equation in the vicinity of a fixed point, where it effectively behaves as a linear map. Then, the behavior close to a fixed point depends on the slope of the function $V_{n+1} = f(V_n)$ [defined by Eq. (11)] at that point. If the absolute value of the slope is smaller than 1, the fixed point is stable and the solutions converge toward it. Otherwise, the fixed point is unstable and the solutions diverge away from it. The solutions are monotonic if the slope is positive, whereas they alternate on each side of the fixed point if it is negative. We can explicitly calculate the derivative of f from Eq. (11), resulting in

$$f'(V) = f(V)\left[\frac{1}{V} - \frac{r\alpha T_b}{|\omega_{ext} - \alpha V| + \omega_c}\right]. \tag{14}$$

If we evaluate Eq. (14) at $V^*_0 = 0$, we find $f'(0) = (1 + \omega_{ext}/\omega_c)^{r(T_b+T_i)} > 1$, indicating that this fixed point is always unstable. The slope at the nonzero fixed point $V^*_{\log}$ is instead given by [Fig. 12(b)]

$$f'(V^*_{\log}) = 1 - rT_b\left(1 + \frac{\Omega - 1}{(\Omega+1)^{\rho}}\right). \tag{15}$$

We thus find that the stability of this fixed point is independent of the feedback gain α, analogous to what we found for continuous swimming in Sec. III C. The fixed point can still become unstable when $f'(V^*_{\log}) < -1$, which can happen for large values of rT_b. The instability boundary depends on the values of Ω and ρ. For $\Omega \to 0$, $f'(V^*_{\log}) \to 0$ independently of ρ. For $\Omega \to \infty$, $f'(V^*_{\log}) \to -\infty$ for $\rho < 1$ and $f'(V^*_{\log}) \to 1 - rT_b$ for $\rho > 1$.

We can also numerically simulate the system by choosing an initial condition V_0 and iteratively evaluating Eq. (11). To illustrate the range of possible behaviors, we plotted solutions for different values of rT_b, together with the corresponding cobweb constructions (Fig. 13). As the slope at the fixed point $f'(V^*_{\log})$ is increased, one first observes monotonic and then alternating convergence to $V^*_{\log}$. Eventually, the fixed point becomes unstable, however, as opposed to the linear system, the solutions do not diverge to infinity but instead exhibit either periodic trajectories or chaotic behavior.

To investigate the existence of such periodic trajectories, we studied the behavior of the second iterate $f^2(V)$, while varying the three independent parameters Ω, ρ, and rT_b. In addition to the fixed points of $f(V)$, we found other fixed points that appear when rT_b becomes sufficiently large. These points correspond to period-2 cycles, that is, oscillatory trajectories in which the swimming speed alternates between two different values. Such solutions can appear even before $V^*_{\log}$ becomes unstable, resulting in a situation where multiple attractors coexist and the long-term behavior of the solutions depends on the initial condition. Further increasing rT_b, we also found additional fixed points of the third iterate $f^3(V)$, corresponding to period-3 cycles. The existence of a period-3 cycle then implies the simultaneous presence of cycles of all other periods and of chaotic behavior [50].

We constructed a bifurcation diagram of the system by simulating it over a range of values of rT_b and plotting the swimming speeds that are visited by the solutions after an initial transient (Fig. 14). These points indicate the attractors of the system as a function of rT_b, that is, the sets of values

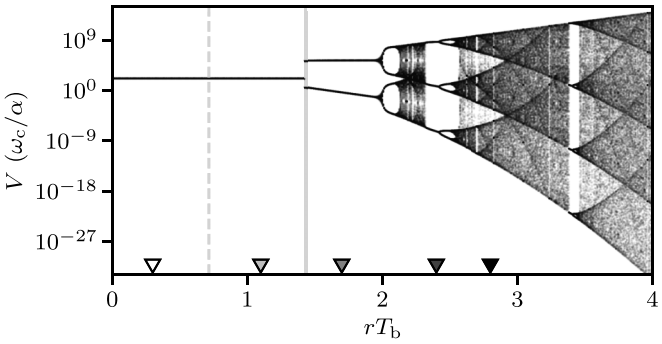

FIG. 14. Bifurcation diagram showing the attractors of Eq. (11) as a function of rT_b. It is obtained by plotting the points visited by the solutions of the equation after an initial transient. The triangles indicate the values of rT_b used in the examples of Fig. 13, the other parameters are the same as in that figure.

explored by the dynamics in the long-time limit. Initially, as rT_b is increased, the attractors change from a single stable fixed point to two distinct values, corresponding to a period-2 cycle. At larger values of rT_b, we observe different intervals either containing a finite number of curves, corresponding to cycles of different periods, or bands densely populated with points, corresponding to chaotic attractors. We will see that the parameters of the model in the case of zebrafish correspond to the regime with a single stable fixed point, so that periodic or chaotic trajectories are not observed in practice. Moreover, such trajectories can span several orders of magnitude in swimming speed (see Fig. 13), but we expect the model to break down outside the limited range of swimming speeds physiologically accessible to the fish.

E. Interpretation of experiments in zebrafish

Having analyzed the behavior of the model, we now examine whether it reproduces the experimental observations on the optomotor response in zebrafish larvae. To get an idea of the behavior of the model without fine-tuning its parameters, we decided to consider the values of r and ω_c that were estimated for danionella (see Sec. III C), rather than finding the values that best fitted the data. Then, using the typical value of T_b observed in zebrafish (see Sec. IV A), we obtain $rT_b \approx 0.3$. The other two dimensionless parameters, ρ and Ω, are linked together by the interbout dynamics through $T_i = \Phi_i/\ln(\omega_{ext}/\omega_{th})$, as described in Sec. IV B (see curves in Fig. 12). Then, for a given value of the external flow rate ω_{ext}, we can estimate all of the three dimensionless parameters that characterize the dynamics of Eq. (11).

For ω_{ext} in the range 0.1–10 rad/s, we find that the slope of the map at the fixed point $f'(V^*_{log})$ [Eq. (15)] remains in the range 0.3–0.7, corresponding to a monotonic convergence to the fixed point (Fig. 13, left). In this regime, for fixed values of α and ω_{ext}, the bout speed converges to the fixed point V^*_{log} and the fish keeps swimming at that speed indefinitely.

In Sec. IV C, we have shown that a linear feedback controller [Eq. (7)] leads to an instability for large values of the feedback gain α, something that was not addressed before by studies that proposed models of this kind [24]. Then, in Sec. IV D, we demonstrated that logarithmic transformations [Eq. (10)] prevent this instability by making the stability of the system independent of α. Because of this, the parameters of the system can be chosen such that it remains both stable and responsive in the physiologically relevant range of ω_{ext}, similarly to our discussion of the continuous case (see Sec. III C).

1. Positional stabilization

We have seen that, while the fixed point of the linear system V^*_{lin} [Eq. (8)] corresponds to a perfect positional stabilization, the fixed point of the nonlinear system V^*_{log} [Eq. (12)] can correspond to an imperfect stabilization, as quantified by their ratio $\eta = V^*_{log}/V^*_{lin}$ [Eq. (13)]. For our estimates of the parameters, we find that increasing ω_{ext} from 0.2 to 8 rad/s leads to a decrease of η from 4 to 1 [see Fig. 12(a)], with $\eta > 1$ corresponding to a forward drift of the fish.

While some experiments in zebrafish have reported an imperfect stabilization and a net drift in the position of the fish [24], which could be partially explained by the predictions of the nonlinear model, others report perfect stabilization [38], suggesting that another mechanism might be at play. Similarly to what we observed for danionella in Sec. III E, we could expect an additional mechanism that integrates the optic flow rate ω on a longer timescale and corrects an eventual positional drift. As the imperfect stabilization results from the compressed representation of the flow rate, the drift correction term would have to be proportional to the integral of ω, rather than to that of S as in Sec. III E. If we add an additional term of the form $r\lambda_c \int_0^t \omega(t')dt'$ to the evolution of the motor drive, then Eq. (11) is modified in the following way:

$$V_{n+1} = f(V_n)e^{r\lambda_c \int_{t_n}^{t_{n+1}} \int_0^t \omega(t')dt'dt}. \tag{16}$$

We find an additional multiplicative factor that depends on the integral of the optic flow rate. If the parameter λ_c is small, this additional factor does not significantly influence the dynamics of Eq. (11) over short timescales, but it accumulates a net positional drift and corrects the swimming speed to eliminate any such drift over long timescales. Thus, introducing such a drift correction term shifts the fixed point of the equation from V^*_{log} to V^*_{lin}, leading to a perfect positional stabilization without significantly changing the short-term dynamics of the bout speed studied in Sec. IV D.

We can simulate the system for a range of different values of ω_{ext} and α to compare the positional stabilization with and without drift correction. Up to this point, we considered deterministic dynamics for the swimming speed. However, as the behavior of the fish is inherently stochastic, we first extend the model to include two different sources of stochasticity, leading to fluctuations in the interbout duration and in the bout speed. A first source of noise comes in by considering the interbout duration $T_{i,n}$ after each swimming bout as a lognormally distributed random variable, rather than just using its typical value as we have done so far (see Sec. III D). To get the interbout duration for each swimming bout, we sample the lognormal distribution $T_{i,n} \sim \text{Lognormal}(\ln(\Phi_i/\ln(\omega_{ext}/\omega_{th})), \sigma_i^2)$. Additionally, we can consider another source of noise in the evolution of the motor drive M, that until now we took to be deterministic. Similarly to Ref. [35], we add a Gaussian white noise term with amplitude σ_ξ to the rate of change of M. Integrating this

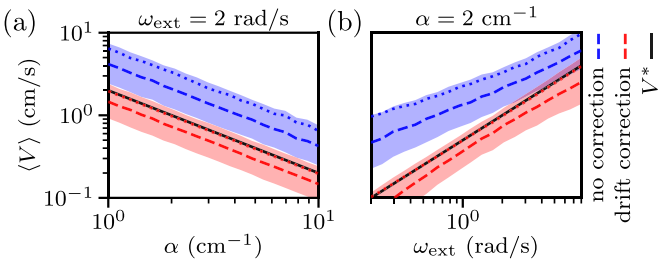

FIG. 15. Net speed per bout $\langle V \rangle$ from stochastic simulations of Eq. (11) (dashed lines and shaded areas indicate the quartiles of the distributions across $N = 10^4$ bouts, whereas dotted lines indicate the mean), compared with the target speed $V^* = \omega_{ext}/\alpha$ (black solid lines). Simulations were performed either with a drift correction term [red, $\lambda_c = 0.01$, Eq. (16)] or without it (blue). Stochasticity is included both in the evaluation of interbout duration ($\sigma_i = 0.3$) and bout speed [$\sigma_\xi = 0.9\,\mathrm{s}^{-1/2}$, Eq. (17)]. (a) For different values of the feedback gain α and $\omega_{ext} = 2$ rad/s, as in Refs. [20,21]. (b) For different values of the external flow rate ω_{ext} and $\alpha = 2\,\mathrm{cm}^{-1}$, as in Ref. [38].

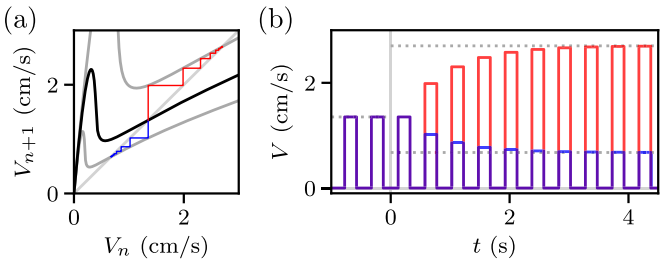

FIG. 16. System response to changes of the feedback gain. (a) Cobweb constructions showing the evolution of the swimming speed according to Eq. (11) (black line) when the feedback gain is changed from $\alpha_0 = 5\,\mathrm{cm}^{-1}$ to either $\alpha_{1,+} = 10\,\mathrm{cm}^{-1}$ (blue lines) or $\alpha_{1,-} = 2.5\,\mathrm{cm}^{-1}$ (red lines). Parameter values: $\omega_{ext} = 2$ rad/s, $T_b = 0.2$ s, and $T_i = 0.25$ s. (b) Swimming speed traces over time corresponding to the two solutions shown in panel (a), showing how the bout speed progressively changes over several bouts from the original fixed point to the shifted ones (dotted lines) after the feedback gain is changed (at $t = 0$).

stochastic term in time from one bout to the next, we obtain a multiplicative noise factor in Eq. (11):

$$V_{n+1} = f(V_n)e^{\sigma_\xi \sqrt{T_b + T_{i,n}}\xi_n}, \tag{17}$$

where $\xi_n \sim \mathcal{N}(0, 1)$ is a unit Gaussian random variable. Taking into account both sources of noise, we can numerically simulate trajectories of the swimming speed by starting with some initial condition V_0 and then sampling the interbout duration $T_{i,n}$ and the noise ξ_n for each bout and evaluating the swimming speed V_{n+1} at the following bout. To perform the simulations, we considered the value $\sigma_\xi \approx 0.9\,\mathrm{s}^{-1/2}$ that was estimated for danionella in Ref. [35] and we estimated $\sigma_i \approx 0.3$ from the standard deviation of $\ln(T_i)$ in zebrafish in Ref. [38].

Given that T_i is now varying from bout to bout, we cannot simply look at the bout speed V_b to evaluate whether the solutions correspond to a stabilization of the fish position. Instead, we calculate the net speed per bout $\langle V \rangle$ including the duration of a swimming bout and the following resting period as $\langle V \rangle = V_b/(1 + \rho)$. We numerically simulated trajectories for different values of ω_{ext} and α, matching those used in the experiments of Refs. [20,21,38], and looked at the resulting distribution of the net speed per bout $\langle V \rangle$. For stochastic simulations without drift correction (Fig. 15, blue), the net speed of the fish varies with the target speed $V^* = \omega_{ext}/\alpha$, but exceeds the target across the range of parameters considered. We see that the discrepancy decreases as ω_{ext} increases, in accordance with our estimates of η over this range [Fig. 12(a)]. As expected, including the drift correction term of Eq. (16) (Fig. 15, red) results in a net speed $\langle V \rangle$ that matches the target V^* on average, corresponding to a perfect positional stabilization. Despite its effect on long-term stabilization, we do not include the drift correction term in the following for simplicity, as it does not significantly influence the short-term dynamics of the system.

2. Dynamics of adaptation

Experiments in Ref. [21] have shown that, after a change in feedback gain, the bout speed changes gradually over several bouts. While such a gradual adaptation has been interpreted as motor learning of the altered feedback gain, here we show that it can arise from the dynamics of the nonlinear feedback controller we studied in Sec. IV D. We consider the evolution of the bout speed V_b according to Eq. (11). We have seen that, for our estimates of the parameters and across a wide range of ω_{ext}, the fixed point V^*_{log} is stable, as the slope $f'(V^*_{log})$ lies between 0 and 1. We consider a system with feedback gain α_0 to be in its steady state, with bout speed equal to $V^*_{log,0}$, and study the evolution of the speed after a sudden change of the feedback gain to a different value α_1 (Fig. 16). Looking at Eq. (11), we see that changing α is equivalent to rescaling the swimming speed. Then, the map controlling the dynamics of the speed becomes $f_1(V) = \frac{\alpha_0}{\alpha_1} f_0(\frac{\alpha_1}{\alpha_0}V)$ and the fixed point moves to $V^*_{log,1} = \frac{\alpha_0}{\alpha_1} V^*_{log,0}$. As the slope $f'(V^*_{log})$ is independent of α, the shifted fixed point is also stable and the bout speed converges to it. The convergence rate is approximately given by $f'(V^*_{log})$, since the function $f(V)$ can be reasonably approximated by its linearization around the fixed point. Therefore, the bout speed converges exponentially to the shifted fixed point, reaching 90% of the way after $\approx 1 - \log_{10}(f'(V^*_{log}))^{-1}$ bouts. If we consider $\omega_{ext} = 2$ rad/s, as in the experiments of Ref. [21], we find that it converges after ≈ 5 bouts, which matches the adaptation timescale observed experimentally.

We note that for linear control [Eq. (7)], the convergence rate depends on the feedback gain and the system becomes unstable if α is larger than a critical value. In contrast, the nonlinear transformations included in Eq. (10) make the system adaptive, such that the convergence rate is independent of α.

3. Directional asymmetry in responsiveness

In Refs. [24,25], it was suggested that the fish only modulate their locomotion based on the forward optic flow corresponding to the external current, effectively disregarding

the backward optic flow corresponding to visual feedback. However, such an interpretation cannot explain the ability of the fish to stabilize their position in different conditions, as the target speed depends not only on the external flow rate ω_{ext}, but also on the feedback gain α. Specifically, a linear feedback model was used to fit the experimental data, with different responsiveness values, k_+ and k_-, for forward and backward flows, respectively. The fitting procedure yielded a large value of the ratio k_+/k_-, which was interpreted as indicating that swimming speed is mainly determined by forward flows [24].

Here, we show that the nonlinearities in our model [Eq. (10)] can give rise to an asymmetry in the effective responsiveness to forward and backward flows, even though the response function itself is symmetric. To compare the dynamics of the nonlinear model with those of the linear model [Eq. (7)], we can linearize Eq. (10) around the fixed point $V^*_{\log}$. Then, the values of k_+ and k_- can be read off from the two terms in the update of the swimming speed, which are proportional to T_{i} and T_{b}, respectively. We find $k_\pm = rV^*_{\log}\ln^*(\omega_\pm/\omega_{\text{c}})/\omega_\pm$, with $\omega_+ = \omega_{\text{ext}}$ and $\omega_- = \omega_{\text{ext}} - \alpha V^*_{\log}$. Finally, using the expression for the fixed point $V^*_{\log}$ [Eq. (12)], we obtain the following responsiveness ratio:

$$\frac{k_+}{k_-} = \frac{(1+\Omega)^\rho - 1}{\rho\Omega}. \tag{18}$$

We see that $k_+/k_- > 1$ for $\rho > 1$, whereas $k_+/k_- < 1$ for $\rho < 1$. This is because for $\rho > 1$ the interbout lasts longer than the bout and thus the fish needs to swim at large speeds to compensate for the forward optic flow accumulated during the interbout interval, resulting in $|\omega_-| > |\omega_+|$. As the rate of change of the motor drive depends on the logarithm of the optic flow rate, which is a sublinear function of ω, the estimated linear responsiveness decreases with ω. Thus, if the flow rate during the bout is larger in magnitude than that during the interbout period $|\omega_-| > |\omega_+|$, then the backward responsiveness is smaller than the forward one $k_- < k_+$. Considering interbout durations corresponding to values of ω_{ext} in the range 0.1–1 rad/s [see Fig. 10(a)], we obtain responsiveness ratios k_+/k_- in the range 3–7.

This shows that interpreting the dynamics of the nonlinear system through a linear model with asymmetric responsiveness can give the misleading impression that the fish is more sensitive to forward than backward flows. In fact, the apparent asymmetry arises from the nonlinear compression of flow rate combined with the different durations of swimming and resting periods. It is important to note that this effect does not justify disregarding the response to backward flows. This is because the smaller responsiveness to backward flows arises from the larger backward flow rate observed when $T_{\text{b}} < T_{\text{i}}$, which compensates for the effect of the reduced responsiveness in determining the swimming speed.

4. Different integration timescales

Finally, we show that our model naturally gives rise to different integration timescales, because of the fact that bout initiation and bout speed are governed by distinct processes. As a result, it can account for the observations of Ref. [25] without the need to introduce a model that explicitly includes two distinct integration timescales. In that work, the authors first considered a current with a randomly switching direction and used reverse correlation to estimate the bout-triggered average stimulus, finding an exponential decay with a time constant of ≈3 s. They showed that this time constant could not be explained by a memoryless Poisson process for bout initiation, for which the decay would only depend on the switching rate of the stimulus. In contrast, our integrate-to-threshold mechanism for bout initiation (see Sec. IV B) leads to a first-passage problem for a random walk driven by the stochastically switching current direction, resulting in a longer characteristic timescale determined not only by the statistics of the stimulus but also by the dynamics of the integration mechanism. In a different experiment, they showed that the swimming speed in response to closed-loop currents depends on the direction of a preceding open-loop current, even after a long pause of 16 s. This second observation is consistent with our proposed mechanism for bout speed selection (see Sec. IV D), which depends on the sensory drive integrated over time, without any leak term. The motor drive is either increased or decreased depending on the two possible directions of open-loop current, which correspond to opposite signs of the sensory drive. This difference in motor drive leads to the observed difference in swimming speed in response to the following closed-loop current. To be precise, we could actually expect a small leak term to be present in the dynamics of the motor drive, which we have ignored until now to keep the model as simple as possible. Such a term would slowly drive M back to zero in the absence of sensory drive, accounting for the gradual decay observed in the effect of the open-loop current as the pause duration increases. We note that our interpretation of the results does not imply that the fish maintain a memory of their location in the environment, as suggested in Ref. [22], but only that they integrate the perceived optic flow rate over time, a mechanism compatible with the neural activity observed in that study.

V. DISCUSSION

In this paper, we studied how the logarithmic encoding of physical variables in the brain can lead to robust positional stabilization through simple feedback control of motor output based on visual input. Such logarithmic encoding is a fundamental feature of nervous systems, widespread across the animal kingdom. At the sensory end it is known as the Weber-Fechner law [36], while at the motor end it corresponds to Henneman's size principle [37]. Although these two principles have often been discussed in terms of informational efficiency [51–53], here we have shown how they jointly contribute to sensorimotor computations. Our results demonstrate that these nonlinear sensorimotor transformations naturally result in an adaptive responsiveness to different contexts, that is, different relationships between motor output and reafferent visual feedback. This emergent adaptation prevents the dynamical instabilities that could otherwise arise because the response of any animal is inherently constrained by temporal delays between perception and action. Such delays originate from finite processing times within the sensorimotor loop and, in many species, from the intermittent or cyclic nature of locomotion.

These ideas were first introduced in Ref. [35], which studied the optomotor response in danionella larvae, where the continuous modulation of swimming made it straightforward to infer the underlying sensorimotor transformations. Although visuomotor stabilization has been extensively studied in larval zebrafish, the underlying mechanisms have remained elusive due to the intermittent nature of their swimming. Behavioral readouts are available only during discrete swimming bouts, obscuring the continuous processes that contribute to stabilization. Here, we have extended the concepts originally developed for danionella to formulate a mathematical framework for visuomotor stabilization, applicable to both continuous and intermittent locomotion.

In the continuous case, we obtained a delay differential equation describing the evolution of the speed and identified a potential instability arising from the delays in the sensorimotor loop. We showed how logarithmic transformations prevent this instability by making the dynamics multiplicative and limiting the responsiveness of the system, such that the stability becomes independent of the feedback gain and the solutions remain confined to limit cycles. We further analyzed the experimental data in danionella, modeling the initiation of swimming as an accumulation process that integrates the sensory drive up to a threshold. Finally, we identified an integration mechanism that compensates for positional drift.

In the intermittent case, we derived a difference equation for the speed and identified an instability analogous to the continuous case, but arising from the delays in between discrete locomotor events. Again, logarithmic transformations make the stability of the system independent of the feedback gain, depending only on parameters intrinsic to the animal and not on the environmental context. We used this framework to interpret the experimental evidence from the visuomotor literature on zebrafish larvae. Our model reproduced many experimental observations while remaining simple and using only a few parameters. Remarkably, using the same response function estimated for danionella, we still obtained results that closely match the observations in zebrafish.

Both danionella and zebrafish larvae allow for whole-brain functional imaging at cellular resolution and are used as model organisms in systems neuroscience to study how sensorimotor computations are implemented at the level of the neural activity [26,54]. While this approach offers insight into the neural circuits underlying these behaviors, the high dimensionality of the recorded data and the limited temporal resolution of current imaging techniques make it challenging to directly infer the sensorimotor transformations [16,55,56]. This is evident from the fact that, although many of the studies described in Sec. II B recorded neural activity alongside visuomotor behavior in larval zebrafish, they still reached different conclusions regarding the mechanisms underlying stabilization [21–23,25,38].

While we applied this theory to explain visuomotor stabilization in two fish species, we expect it to be readily applicable to other animals. This is because such visuomotor reflexes [11,57,58], along with the principles of logarithmic coding [59], are found across many different species and contexts. In engineering, designing control mechanisms that rely solely on visual input remains notoriously difficult, and additional sensors are typically used to disentangle speed and distance from the measured optic flow [10,60]. Our model, however, could be implemented as a simple algorithm that first compresses logarithmically the inputs and then decompresses them to generate the output. We suggest that this approach could enable robust stabilization in flying or swimming robots subjected to unpredictable external perturbations.

ACKNOWLEDGMENTS

I thank the members of the Laboratoire Jean Perrin and the SmartNets European Training Network, especially Georges Debrégeas and Monica Coraggioso, for helpful feedback and discussions. This work was supported by the European Union's Horizon 2020 research and innovation programme under the Marie Skłodowska-Curie Grant Agreement No. 860949 and by the Agence Nationale de la Recherche under the Locomat Project No. ANR-21-CE16-0037.

DATA AVAILABILITY

The data that support the findings of this article are openly available [61,62].

[1] M. F. Land and D.-E. Nilsson, *Animal Eyes*, 2nd ed., Oxford Animal Biology Series (Oxford University Press, Oxford, 2012).

[2] J. J. Gibson, Visually controlled locomotion and visual orientation in animals, Br. J. Psychol. **49**, 182 (1958).

[3] R. Shadmehr, M. A. Smith, and J. W. Krakauer, Error correction, sensory prediction, and adaptation in motor control, Annu. Rev. Neurosci. **33**, 89 (2010).

[4] S. G. Tzafestas, Mobile robot control and navigation: A global overview, J. Intell. Robot. Syst. **91**, 35 (2018).

[5] R. C. Miall and D. M. Wolpert, Forward models for physiological motor control, Neural Networks **9**, 1265 (1996).

[6] M. Kawato, Internal models for motor control and trajectory planning, Curr. Opin. Neurobiol. **9**, 718 (1999).

[7] C. Tin and C.-S. Poon, Internal models in sensorimotor integration: Perspectives from adaptive control theory, J. Neural Eng. **2**, S147 (2005).

[8] D. Nguyen-Tuong and J. Peters, Model learning for robot control: A survey, Cogn. Process. **12**, 319 (2011).

[9] J. J. Koenderink, Optic flow, Vision Res. **26**, 161 (1986).

[10] J. R. Serres and F. Ruffier, Optic flow-based collision-free strategies: From insects to robots, Arthropod Struct. Dev. **46**, 703 (2017).

[11] M. V. Srinivasan and S. Zhang, Visual motor computations in insects, Annu. Rev. Neurosci. **27**, 679 (2004).

[12] G. P. Arnold, Rheotropism in fishes, Biol. Rev. **49**, 515 (1974).

[13] G. D. McCann, G. F. MacGinitie, and J. W. S. Pringle, Optomotor response studies of insect vision, Proc. Roy. Soc. London Ser. B **163**, 369 (1997).

[14] E. Shaw and A. Tucker, The optomotor reaction of schooling carangid fishes, Anim. Behav. **13**, 330 (1965).

[15] R. Portugues and F. Engert, The neural basis of visual behaviors in the larval zebrafish, Curr. Opin. Neurobiol. **19**, 644 (2009).

[16] M. B. Orger and G. G. d. Polavieja, Zebrafish behavior: Opportunities and challenges, Annu. Rev. Neurosci. **40**, 125 (2017).

[17] J. H. Bollmann, The zebrafish visual system: From circuits to behavior, Annu. Rev. Vis. Sci. **5**, 269 (2019).

[18] M. B. Ahrens, M. B. Orger, D. N. Robson, J. M. Li, and P. J. Keller, Whole-brain functional imaging at cellular resolution using light-sheet microscopy, Nat. Methods **10**, 413 (2013).

[19] T. Panier, S. A. Romano, R. Olive, T. Pietri, G. Sumbre, R. Candelier, and G. Debrégeas, Fast functional imaging of multiple brain regions in intact zebrafish larvae using Selective Plane Illumination Microscopy, Front. Neural Circuits **7**, 65 (2013).

[20] R. Portugues and F. Engert, Adaptive locomotor behavior in larval zebrafish, Front. Syst. Neurosci. **5**, 72 (2011).

[21] M. B. Ahrens, J. M. Li, M. B. Orger, D. N. Robson, A. F. Schier, F. Engert, and R. Portugues, Brain-wide neuronal dynamics during motor adaptation in zebrafish, Nature (London) **485**, 471 (2012).

[22] E. Yang, M. F. Zwart, B. James, M. Rubinov, Z. Wei, S. Narayan, N. Vladimirov, B. D. Mensh, J. E. Fitzgerald, and M. B. Ahrens, A brainstem integrator for self-location memory and positional homeostasis in zebrafish, Cell **185**, 5011 (2022).

[23] D. A. Markov, L. Petrucco, A. M. Kist, and R. Portugues, A cerebellar internal model calibrates a feedback controller involved in sensorimotor control, Nat. Commun. **12**, 6694 (2021).

[24] J. G. Holman, W. W. K. Lai, P. Pichler, D. Saska, L. Lagnado, and C. L. Buckley, A behavioral and modeling study of control algorithms underlying the translational optomotor response in larval zebrafish with implications for neural circuit function, PLoS Comput. Biol. **19**, e1010924 (2023).

[25] R. Tanaka and R. Portugues, Algorithmic dissection of optic flow memory in larval zebrafish, Curr. Biol. **35**, 4870 (2025).

[26] L. Schulze, J. Henninger, M. Kadobianskyi, T. Chaigne, A. I. Faustino, N. Hakiy, S. Albadri, M. Schuelke, L. Maler, F. Del Bene, and B. Judkewitz, Transparent *Danionella translucida* as a genetically tractable vertebrate brain model, Nat. Methods **15**, 977 (2018).

[27] R. Britz, K. W. Conway, and L. Rüber, The emerging vertebrate model species for neurophysiological studies is *Danionella cerebrum*, new species (Teleostei: Cyprinidae), Sci. Rep. **11**, 18942 (2021).

[28] M. Hoffmann, J. Henninger, J. Veith, L. Richter, and B. Judkewitz, Blazed oblique plane microscopy reveals scale-invariant inference of brain-wide population activity, Nat. Commun. **14**, 8019 (2023).

[29] T. J. Lee and K. L. Briggman, Visually guided and context-dependent spatial navigation in the translucent fish *Danionella cerebrum*, Curr. Biol. **33**, 5467 (2023).

[30] V. A. N. O. Cook, A. H. Groneberg, M. Hoffmann, M. Kadobianskyi, J. Veith, L. Schulze, J. Henninger, R. Britz, and B. Judkewitz, Ultrafast sound production mechanism in one of the smallest vertebrates, Proc. Natl. Acad. Sci. USA **121**, e2314017121 (2024).

[31] J. Veith, T. Chaigne, A. Svanidze, L. E. Dressler, M. Hoffmann, B. Gerhardt, and B. Judkewitz, The mechanism for directional hearing in fish, Nature (London) **631**, 118 (2024).

[32] D. Zada, L. Schulze, J.-H. Yu, P. Tarabishi, J. L. Napoli, J. Milan, and M. Lovett-Barron, Development of neural circuits for social motion perception in schooling fish, Curr. Biol. **34**, 3380 (2024).

[33] A. H. Groneberg, L. E. Dressler, M. Kadobianskyi, J. Müller, and B. Judkewitz, Development of sound production in *Danionella cerebrum*, J. Exp. Biol. **227**, jeb247782 (2024).

[34] G. Rajan, J. Lafaye, G. Faini, M. Carbo-Tano, K. Duroure, D. Tanese, T. Panier, R. Candelier, J. Henninger, R. Britz, B. Judkewitz, C. Gebhardt, V. Emiliani, G. Debregeas, C. Wyart, and F. Del Bene, Evolutionary divergence of locomotion in two related vertebrate species, Cell Rep. **38**, 110585 (2022).

[35] L. Demarchi, M. Coraggioso, A. Hubert, T. Panier, G. Morvan-Dubois, V. Bormuth, and G. Debrégeas, Logarithmic coding leads to adaptive stabilization in the presence of sensorimotor delays, Proc. Natl. Acad. Sci. USA **122**, e2510385122 (2025).

[36] J. C. Baird and E. J. Noma, *Fundamentals of Scaling and Psychophysics* (Wiley, New York, 1978).

[37] E. Henneman, Relation between size of neurons and their susceptibility to discharge, Science **126**, 1345 (1957).

[38] K. E. Severi, R. Portugues, J. C. Marques, D. M. O'Malley, M. B. Orger, and F. Engert, Neural control and modulation of swimming speed in the larval zebrafish, Neuron **83**, 692 (2014).

[39] R. Portugues, M. Haesemeyer, M. L. Blum, and F. Engert, Whole-field visual motion drives swimming in larval zebrafish via a stochastic process, J. Exp. Biol. **218**, 1433 (2015).

[40] T. W. Dunn and J. E. Fitzgerald, Correcting for physical distortions in visual stimuli improves reproducibility in zebrafish neuroscience, eLife **9**, e53684 (2020).

[41] S. D. Brown and A. Heathcote, The simplest complete model of choice response time: Linear ballistic accumulation, Cognit. Psychol. **57**, 153 (2008).

[42] C. Donkin and L. Van Maanen, Piéron's law is not just an artifact of the response mechanism, J. Math. Psychol. **62-63**, 22 (2014).

[43] G. Buzsáki and K. Mizuseki, The log-dynamic brain: How skewed distributions affect network operations, Nat. Rev. Neurosci. **15**, 264 (2014).

[44] R. Ulrich and J. Miller, Information processing models generating lognormally distributed reaction times, J. Math. Psychol. **37**, 513 (1993).

[45] M. Coraggioso, L. Demarchi, R. Wong, V. Dichio, C. Chaumeton, T. Panier, G. Morvan-Dubois, G. Goodhill, V. Bormuth, and G. Debrégeas, A sensorimotor instability drives a locomotor transition during fish development, bioRxiv.

[46] R. E. Johnson, S. Linderman, T. Panier, C. L. Wee, E. Song, K. J. Herrera, A. Miller, and F. Engert, Probabilistic models of larval zebrafish behavior reveal structure on many scales, Curr. Biol. **30**, 70 (2020).

[47] G. L. Goc, J. Lafaye, S. Karpenko, V. Bormuth, R. Candelier, and G. Debrégeas, Thermal modulation of zebrafish exploratory statistics reveals constraints on individual behavioral variability, BMC Biol. **19**, 208 (2021).

[48] D. Clift, H. Richendrfer, R. J. Thorn, R. M. Colwill, and R. Creton, High-throughput analysis of behavior in zebrafish larvae: Effects of feeding, Zebrafish **11**, 455 (2014).

[49] S. Elaydi, *An Introduction to Difference Equations*, 3rd ed., Undergraduate Texts in Mathematics (Springer, New York, 2005).

[50] T.-Y. Li and J. A. Yorke, Period three implies chaos, Am. Math. Mon. **82**, 985 (1975).

[51] H. Hatze, A teleological explanation of Weber's law and the motor unit size law, Bull. Math. Biol. **41**, 407 (1979).

[52] W. Senn, K. Wyler, H. P. Clamann, J. Kleinle, H. R. Lüscher, and L. Müller, Size principle and information theory, Biol. Cybern. **76**, 11 (1997).

[53] R. D. Portugal and B. F. Svaiter, Weber-Fechner law and the optimality of the logarithmic scale, Minds Mach. **21**, 73 (2011).

[54] R. W. Friedrich, G. A. Jacobson, and P. Zhu, Circuit neuroscience in Zebrafish, Curr. Biol. **20**, R371 (2010).

[55] T. Rose, P. M. Goltstein, R. Portugues, and O. Griesbeck, Putting a finishing touch on GECIs, Front. Mol. Neurosci. **7**, 88 (2014).

[56] F. Ali and A. C. Kwan, Interpreting in vivo calcium signals from neuronal cell bodies, axons, and dendrites: A review, Neurophotonics **7**, 1 (2019).

[57] F. R. Harden Jones, The reaction of fish to moving backgrounds, J. Exp. Biol. **40**, 437 (1963).

[58] A. S. Mauss and A. Borst, Optic flow-based course control in insects, Curr. Opin. Neurobiol. **60**, 21 (2020).

[59] *Principles of Neural Science*, 6th ed., edited by E. R. Kandel, J. Koester, S. Mack, and S. Siegelbaum (McGraw Hill, New York, 2021).

[60] H. Chao, Y. Gu, and M. Napolitano, A survey of optical flow techniques for robotics navigation applications, J. Intell. Robot. Syst. **73**, 361 (2014).

[61] L. Demarchi, M. Coraggioso, A. Hubert, T. Panier, G. Morvan-Dubois, V. Bormuth, and G. Debrégeas, Data and code—Logarithmic coding leads to adaptive stabilization in the presence of sensorimotor delays, Zenodo (2025), https://doi.org/10.5281/zenodo.15187167.

[62] L. Demarchi, Code—A logarithmic theory of visuomotor stabilization, Zenodo (2026), https://doi.org/10.5281/zenodo.17628539.